CHAPTER 5

Application of atomic force microscopy for food polysaccharides

Lifen Zhang[1], Xiaoyang Sun[2], Shaojuan Lai[1], Fusheng Chen[1] and Hongshun Yang[3,4]

[1]College of Food Science and Technology, Henan University of Technology, Zhengzhou, P. R. China
[2]College of Food and Biological Engineering, Henan University of Animal Husbandry and Economy, Zhengzhou, P. R. China
[3]Department of Food Science and Technology, National University of Singapore, Singapore, Singapore
[4]National University of Singapore (Suzhou) Research Institute, Suzhou Industrial Park,, Suzhou, P. R. China

5.1 Introduction

Binning and Quate developed atomic force microscopy (AFM) in 1986 (Funami, 2010). As a scanning probe microscopy, AFM then opens a new vision in imaging and force measurements. AFM can be used to visualize dispersed or isolated molecules, assemble molecules, supermolecular structures, gel precursors, microgels, and network structures of bulk gels, and determine the polymer chain length distribution and chain flexibility (Sletmoen, Maurstad, Sikorski, Paulsen, & Stokke, 2003). Additionally, AFM can be used to stretch single polysaccharide chains to determine the mechanical fingerprints for reflecting the chemical composition, linkage geometry, and higher order structure of polysaccharides. This single-molecule probe technique can also be used to determine the molecular interactions among polysaccharides (Sletmoen et al., 2003). It has been widely used in polysaccharides research; for example, pectin, cellulose, hemicellulose, carrageenan, gellan gum, xanthan gum, xyloglucan (XG), and so on. AFM has the advantage of offering both air and aqueous environments, which make the samples' behaviors similar to those in actual systems (Funami, 2010). It provides the capacity to detect real-time morphology and reactions of samples at an atomic level. Meanwhile, AFM can be used to directly observe and quantify the heterogeneity of polysaccharides (Funami, 2010).

Fundamentals and Application of Atomic Force Microscopy for Food Research
DOI: https://doi.org/10.1016/B978-0-12-823985-8.00004-9

5.2 Plant polysaccharide

5.2.1 Starch

5.2.1.1 Analysis of morphology and structure properties of starch

Starch, one of the most common natural carbohydrate polymers, is a major component of various crops, and an energy provider in our daily diet. As a raw material, starch has been widely used in the chemical and food industries. The major components of starch are amylose and amylopectin composed of glucose units. Amylose is almost linearly, while amylopectin is highly branched. The diameter of starch granules from different sources varies from 1 to 200 μm, and its gelatinization and retrogradation are critical for its use, particularly in food. These properties depend on the modification of starch, and the interactions between starch and other components. It is necessary to understand the structural changes of starch during processing, which could explain the relationship between the structural and functional properties of starch. Thus, AFM is a strong tool to provide structural perspectives of starch. AFM could be used to obtain topography, frictional force, and phase imaging of starch. The AFM images of cornstarch nanocrystals showed that particle size of 10−150 nm could be achieved in the shape of round-edge platelet-like particles (Javidi, Razavi, & Mohammad Amini, 2019). The sizes of hot distilled water isolated amylose-lipid nanomaterials obtained from pasted native (un-irradiated) high amylose maize starch (HAMS) with 0%, 1.5%, and 5% stearic acid were 5−80, 5−100, and 5−110 nm, respectively (Ocloo, Ray, & Emmambux, 2019).

Starch granule has a relationship with the physicochemical properties of starch. Investigation of structure characteristics of starch granules could benefit understanding the functionality of starch. AFM was used to observe the internal structure and surface morphology of starch granules at the molecular level (Yang et al., 2019). For instance, the differences in the internal structure of banana starch granules with different mature stages indicated that the start of enzymatic hydrolysis of starch varied (Peroni-Okita et al., 2015). The observed surface morphology of starch granules in potato, wheat, rice, and corn was different (Baldwin, Davies, & Melia, 1997; Funami, 2010). The functional properties of starch are closely related to the surface structural characteristics of the granules. Chen et al. (2019) applied AMF to investigate the surface features of fractionated potato starch granules, and the results showed that the surfaces of fractionated granules had "blocklet" structures of different nanoscales.

This indicated that the self-assembly behaviors of amylopectin side chains were different.

AFM also could provide the important roughness parameters [average roughness values (R_q) and root mean square roughness (R_a)] of starch granules surfaces. Higher values of R_q and R_a corresponded to more unevenness of the surface (Fig. 5.1) (Chen et al., 2019). Larger granules

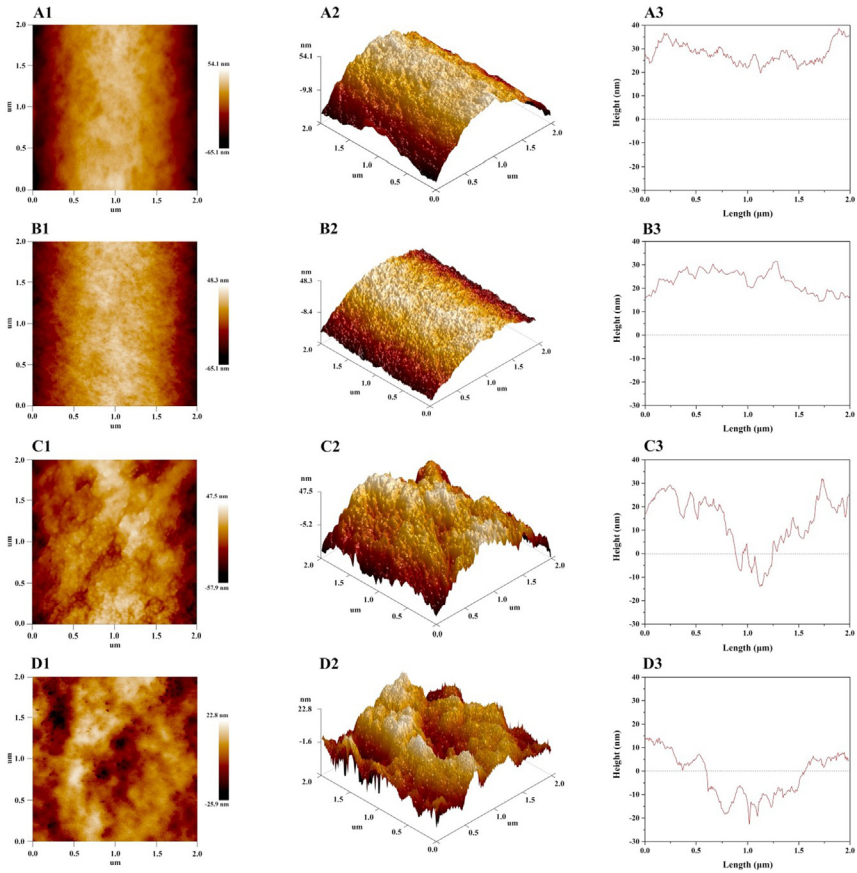

Figure 5.1 Atomic force microscopy scanning of the surface of fractionated potato starch granules. Note: (A1), (B1), (C1) and (D1) topographic images; (A2), (B2), (C2) and (D2) phase images; (A3), (B3), (C3) and (D3) cross section images; (A1, A2, A3) PS-VS; (B1, B2, B3) PS-S; (C1, C2, C3) PS-M; (D1, D2, D3) PS-L. *From Chen, L., Ma, R., Zhang, Z., Huang, M., Cai, C., Zhang, R., McClements, D. J., Tian, Y., & Jin, Z. (2019). Comprehensive investigation and comparison of surface microstructure of fractionated potato starches.* Food Hydrocolloids, 89, 11–19. https://doi.org/10.1016/j.foodhyd.2018.10.017.

with rougher surfaces could easily absorb water and swell. AFM also provides an approach to investigate the starch modification and processing (Wen, Xu, Liu, Corke, & Sui, 2020). AFM imaged the surface of hydrolyzed starches of wheat, corn, and potato, and the results showed that potato and corn starch had similar patterns, while it had different surficial morphology for wheat starch (Tavallaie, Khomeiri, Mousivand, Maghsoudlou, & Hashemi, 2019). Hedayati, Shahidi, Majzoobi, Koocheki, and Farahnaky (2020) investigated the effects of $CaCl_2$ and NaCl on the surface properties of cold water swelling maize starch, and the AFM results showed that NaCl increased the surface wrinkles of starch granules, while $CaCl_2$ reduced the roughness of starch granule surface (Hedayati et al., 2020).

AFM was also applied to investigate the internal structure and biopolymer chains of starch and modified starch. Researchers studied the internal structures of potato, banana, and maize starch granules. The images of maize starch showed a central hole and a radial crack. Globular structures existed within or across the growth rings. The central region of the starch granule of the banana was made up of different materials with different viscoelasticities. Blocklet structures of the size of about 80−200 nm mainly consisted of the central region. Meanwhile, there also existed a few blocklet structures with the size of 15−50 nm in the central region (Chakraborty, Pallen, Shetty, Roy, & Mazumder, 2020; Peroni-Okita et al., 2015; Ridout, Parker, Hedley, Bogracheva, & Morris, 2003).

5.2.1.2 Atomic force microscopy study of starch films

Starch is one of the most biodegradable materials with affordable price, renewability, and wide availability. Starch can be used to produce biodegradable films, and has been widely used in food packaging. The surface properties of films are very important to their mechanical and gas permeability properties. Smooth surfaces can provide a barrier for diffusion of gases and moisture. AFM analysis revealed that ultraviolet (UV)−irradiation method could produce stable bio-thermoplastic films with low surface roughness and high barrier properties. Thus, surface roughness is closely related to film quality (Chandra Mohan, Harini, Karthikeyan, Sudharsan, & Sukumar, 2018). What's more, differences in the microstructure of starches from different sources caused the intermolecular interactions of different intensities during the film formation process, which may lead to the different surface roughness of films. For instance, the surface of cassava, sweet potato, and potato starch films was

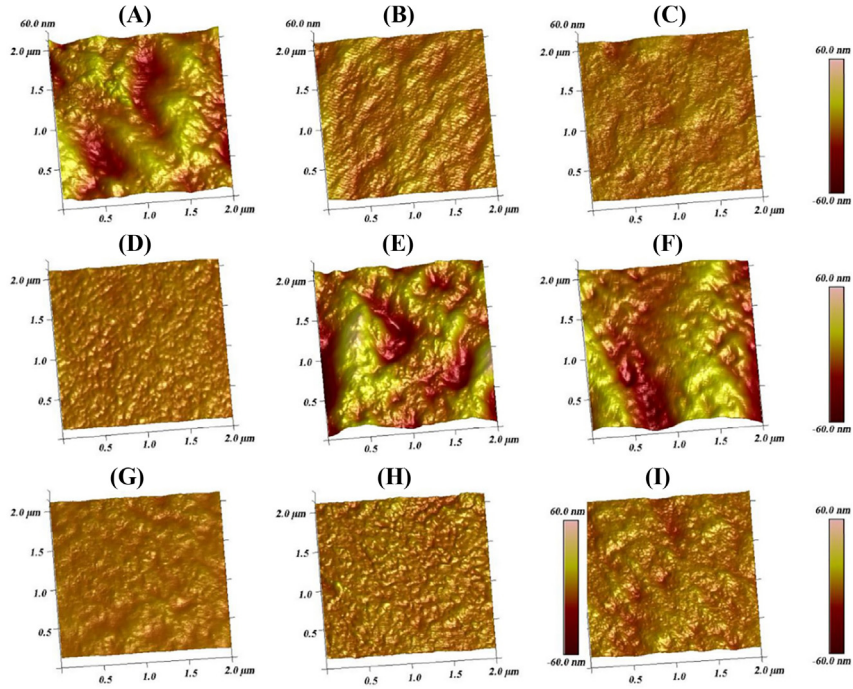

Figure 5.2 Atomic force microscopy topographic images of native starch films (A–F), modified cassava starch films (G–I). Note: (A) WCS film, (B) CAS film, (C) SPS film, (D) PS film, (E) WS film, (F) CS film, (G) ECS film, (H) CCS film, and (I) OCS film. Scan size is 2×2 μm and all figures (A–I) have the same 3D height coordinate scale. Results are expressed as mean ± SD (standard deviation) of three determinations. *From Dai, L., Zhang, J., & Cheng, F. (2019). Effects of starches from different botanical sources and modification methods on physicochemical properties of starch-based edible films.* International Journal of Biological Macromolecules, 132, *897–905. https://doi.org/10.1016/j.ijbiomac.2019.03.197*.

homogeneous except for waxy corn, wheat, and corn starch films (Fig. 5.2) (Dai, Zhang, & Cheng, 2019).

The morphologies of starch films also can be investigated by AFM. Research works applied AFM studied the morphologies of potato starch-olive oil edible films containing zein nanoparticles. The results indicated that R_q of the pure starch film was 30.2, and 34 nm for starch/olive oil film. The addition of zein could increase the smoothness of the film surface. The decrease in surface roughness corresponded to the decrease in water permeability of the film (Farajpour, Emam Djomeh, Moeini, Tavahkolipour, & Safayan, 2020). The microstructure of films prepared using corn/octenylsuccinated starch incorporated with soybean oil in

different concentrations exhibited an irregular and coarse surface, while a smooth and uniform surface was observed in the control film (Gao et al., 2020). According to AFM results, a more compact surface structure of the morphology of bentonite powder modified starch film than that of control was observed. Meanwhile, the average surface roughness of the bentonite-starch film was 21.4 ± 7, and of the control film was 33.4 ± 10 nm (Aguilar-Sánchez et al., 2019).

AFM, as a tool to study the food hydrocolloids, can visualize the gel precursors, microgels, and network structures of bulk gels, and obtain the structural information of food hydrocolloids, such as amylose and starch (Funami, 2010; McIntire & Brant, 1999; Ridout, Gunning, Parker, Wilson, & Morris, 2002). The tapping mode is most suitable for food hydrocolloid analysis. Cai et al. investigated the effects of NaCl on the nanostructure of carboxymethyl starch/xanthan gum combinations stabilized emulsions, and the results confirmed that NaCl caused the extension of the molecular chain of carboxymethyl starch, while the double helix structure of xanthan gum was intertwined with carboxymethyl starch, forming a stable network structure (Cai, Du, Zhu, & Cao, 2020).

5.2.2 Pectin

As a complex anionic polysaccharide, pectin consists of several different *monosaccharides* in various plants (Vincken et al., 2003), and the three polymers of pectin are homogalacturonan (HG), rhamnogalacturonan I (RG I), and rhamnogalacturonan II (RG II). HG and RG I are called "smooth region" and "hairy region," respectively. HG consists of (1,4)-linked α-D-GalA residues. Groups of HG can be methyl esterified or acetylated. The methyl-esterified of HG has great value to the binding capacity, gelation, and rheological behaviors of pectin (Willats, Knox, & Mikkelsen, 2006). This may be covalently cross-linked with RG I through rhamnose (Rha) units. The main bone of RG I consists of alternating GalA and Rha units. RG I also contains side chains including of galactose (Gal) and arabinose (Ara) (Kozioł, Cybulska, Pieczywek, & Zdunek, 2017; Willats, Mccartney, Mackie, & Knox, 2001). RG II is a complex compound that is highly branched (Ishii et al., 1999).

AFM was used to investigate the morphology, degradation, surface manipulation, biomolecular interactions, and mechanical properties of polymers. It also could be used to directly observe the three-dimensional structure of polymers (Magonov & Reneker, 1997). AFM was widely

used to study the nanostructure of pectin. For example, the structural properties of alkali-soluble Canna edulis Ker pectin were evaluated by AFM (Zhang, Cui, Xiao, & Wang, 2014). Meanwhile, pectin degradation of fruits and vegetables during storage also could be investigated by AFM (Yang, Chen, An, & Lai, 2009).

AFM could be used to image the molecules in a liquid, and directly provide information about the height of the molecular chain. It also could be applied to provide information on the contour and branch length, and distribution of the pectin backbone, and be used to observe branch (br), short chain (sc), long chain (lc), the linear single fraction (ls), mutibranch (mbr), and polymer (p) morphologies of pectin chains. Meanwhile, AFM could be useful to determine the single molecules and distinguishing branches of the molecule backbone of overlapping molecules. AFM could provide information about the properties of aggregated structures (Paniagua et al., 2017).

5.2.2.1 Analysis of pectin degradation during cell wall disassembly

As the structural unit of fresh cells and the junction between cells, pectin widely exists in almost all fruit and vegetables (Guo et al., 2014), and accounts up to 60% of cell wall mass. The length, diameter, and branching of pectin play an important role in the texture of fruits. The lengths of pectin polymer and the number of aggregates decreased along with the maturation of fruits (Paniagua et al., 2014). RGII, as the branched structure of pectin, is also important to the cell wall structure (Mohnen, 2008). For the degradation of cell wall polysaccharides, pectin has an obvious effect on the texture change of fruits.

Pectin degradation was due to the change of pectin content and was significantly influenced by the alteration of its nanostructure. Pectin structures affect the stiffness, diffusivity, intercellular cell wall properties, and the macroproperties. Covalently linked pectin is critical to cell walls stiffness during fruit softening. Degradation of pectin in the middle lamella cell wall leads to the decrease of cell-to-cell adhesion, and the stiffening of primary cell walls. During fruit maturation, self-assembly behaviors of the sodium-carbonate soluble pectin (SSP) degraded to a regular gel-like network, which was responsible for the stiffening of primary cell walls (Zdunek, Kozioł, Cybulska, Lekka, & Pieczywek, 2016).

During the ripeness of fruits, softening is mainly related to the dissociation of the middle lamella. The disassembly process of the cell wall has a close relationship to the depolymerization of matrix glycans, the

depolymerization and dissolution of pectin, and the loss of neutral sugars in pectin side chains. Pectin solubilization during fruit ripening may cause the content of acid-water pectin to increase, and the amount of covalently bound pectin to decrease. Thus, the pectin network may be disentangled, and the motility of wall enzymes in the cell wall matrix will be increased. Pectin solubilization could be directly involved in ripe fruits' texture, but its mechanism is unclear. AFM would reveal the changing process of cell wall polymers during softening (Posé et al., 2019).

AFM is a useful tool that was used to observe the structure of plant cell walls in recent years, especially for the changes of pectin during fruit softening. The insights on structural features of pectin and their changes during fruit ripening and postharvest were summarized, and Table 5.1 shows AFM analysis of quality, quantify, and morphology features of pectin during ripening and storage of fruits and vegetables.

Yang et al. introduced AFM to analyze the nanostructures of pectin in fruits for the first time (Yang et al., 2005). They did a series of research on the characterizations including morphology, length, height, and width of pectin nanostructure of peach, apricot, strawberry, cherry, tomato, loquat, red bayberry, winter jujube, and so on. ls, lc, sc, cp, br, mbr, and p morphologies of pectin chains were observed in these fresh fruits. Network also could be observed in calcium-treated fruits (Figs. 5.3 and 5.4).

Quantitative parameters of pectin were different according to the fruit variety and origin. Zhang et al. investigated the widths and lengths of SSP of crisp and soft cherries. The range of widths and lengths were 37−140 nm and 123−1404 nm, respectively. Compared to soft groups, the widths of SSP were larger in crisp groups, but the lengths of SSP in crisp groups were smaller. The relative percentage of wide SSP chains of crisp fruit was higher than that of soft fruit (Zhang et al., 2008). Yang et al. found that the differences in suppleness among three varieties of peaches may own to the different lengths of pectin chains (Yang et al., 2009).The widths and lengths of stone fruits (peach, jujube, and apricot) were also different from each other. The lengths of SSP chain of crisp fruit were mainly within the range of 50−900 nm, while it was 20−100 nm for soft peaches. The main widths of pectin in crisp and soft cultivars were 20−100 nm. Meanwhile, almost all the heights of pectin [chelate-soluble pectin (CSP), water-soluble pectin (WSP), and SSP] were from 1 to 5 nm in the two cultivars (Yang et al., 2009). The pectin chain widths of jujubes were smaller than that of peaches. For unripe jujubes, most of the pectin chain widths were in the range of 47−70 nm. Pectin

Table 5.1 Atomic force microscopy analysis of quality, quantity, and morphology features of pectin from fruits and vegetables during ripening and storage.

Fruits and vegetables (species)	Ripening or storage	Pectin	Nanostructural properties	References
Peach ("Jinxiu," *Prunus persicu* L. Batsch.)	Controlled atmosphere storage	WSP	Linear, branched, blocks, and polymers structures; chain widths were composed of four basic units: 11.719, 15.625, 19.531, and 35.156 nm.	Yang, An, Feng, Li, and Lai (2005)
		CSP	Linear segments, branch points, aggregates, single linear molecule, cleavage points, branch, polymers, linear single fractions, short and long chains, and releasing point structures; widths of chains were composed of four basic units: 17.578, 19.531, 23.438, and 29.297 nm.	Yang, Lai, An, and Li (2006)
		SSP	Linear, branched, blocks, polymers, and large aggregates; widths of chains were composed of four basic units: 11.719, 15.625, 19.531, and 17.578 nm.	Yang, Feng, An, and Li (2006)
Peach (crisp "Jinxiu," and soft "Milu," *Prunus persicu* L. Batsch.)	Cooled for 12 h at 4°C, and stored at 20°C for 6 days	WSP, CSP, and SSP	Aggregates, branched, short and long chains, multiple branched chains, and releasing point structures; widths: about 20−100 nm; heights: about 1−5 nm; lengths: firm peaches, WSP, about 0.3−4.0 μm; CSP, approximately from 0.1 to 3.0 μm; SSP, 249 ± 256 nm ($n = 138$); soft peaches, WSP, 0.8−4.2 μm; CSP, approximately from 0.1 to 3.0 μm; SSP, 57 ± 27 nm ($n = 40$).	Yang et al. (2009)

(*Continued*)

Table 5.1 (Continued)

Fruits and vegetables (species)	Ripening or storage	Pectin	Nanostructural properties	References
Peach ("Cangfangzaosheng" and "Songsenzaosheng," *Prunus persicu* L. Batsch.)	Cold storage	WSP, CSP, and SSP	Polymers, blocks, and single linear chains structures; widths of peach pectin (WSP, CSP, and SSP) were composed of limited basic values.	Zhang et al. (2010, 2012)
Chinese cherry (*Prunus pseudocerasus* L.)	Unripe and ripe	SSP	Linear single fraction, cleavage point, branched, and polymers structures; heights: 1.3−6.8 nm; widths: four basic units 37, 47, 55, and 61 nm; lengths: four basic units 123, 202, and 380 nm.	Zhang et al. (2008)
Apricots ("Jinhong," *P. armeniaca L.*)	Calcium treatment	CSP	Branched, linear single fraction, short and long chains, polymers, releasing point, and cleavage point structures; heights: 0.2−3.0 nm; lengths: 400−3600 nm.	Liu et al. (2009)
	Pectinase treatment	CSP	Branched, linear single fraction, short and long chain, cleavage point, releasing point, and polymer structures; lengths: untreated samples, 0.5−1 μm; pectinase treated samples, 0−1 μm; heights: 0.2−3.0 nm for both control and treated samples.	Chen et al. (2013)
Jujubes ("Huanghua" and "Zhanhua," *Zizyphus jujuba*)	Unripe and ripe	CSP, and SSP	Unripe: CSP widths, 35−60 nm for both cultivars; SSP widths, 35−157 nm for both cultivars; ripe: CSP widths, 15−35 nm for	Wang et al. (2012)

			both cultivars; SSP widths, 15−80 nm for both cultivars.	
Strawberries ("Shijixiang," *Fragaria annanassa* Duch.)	Calcium treatment	WSP, CSP, and SSP	Long and single chains, and multibranched structures; widths: WSP, and CSP, 23−80 nm; SSP, 23−60 nm; lengths: WSP, and SSP mainly in 50−2000 nm.	Chen et al. (2011)
Tomatoes (crisp "Dongsheng" and soft "Geruisi" *Lycopersicon esculentum Mill.*)	Ripening	CSP	Polymers, long chains, linear single fraction, short chains, branched, cleavage points, and releasing point structures; widths: 15−118 nm; heights: 0.5−6 nm.	Xin et al. (2010)
Cherry tomatoes ("Mali," *Lycopersicon esculentum Mill.*)	Rice bran wax coating	CSP	Branched, linear strands, short and long chains, and polymer structures; widths: 15−250 nm; heights: 0.2−2 nm.	Zhang, Chen, Zhang, Lai, and Yang (2017)
Chinese red bayberries ("Lang dangzi," *Myrica rubra Sieb. Et Zucc.*)	Vacuum impregnation combined with calcium ascorbate treatment	CSP	Short and long chains, linear single fractions, branched, polymers, and aggregates structures; widths: fresh, 20−90 nm; lengths: fresh, 100−1200 nm; heights: fresh, 0.5−4.5 nm; larger frequency of CSP chain width and length of samples treated by the combination of vacuum impregnation and calcium ascorbate were observed.	Li, Zhang, Chen, Lai, and Yang (2018)
Winter jujubes ("Nongke I," *Zizyphus jujube Miller.*)	Calcium and pectin methylesterase treatment	WSP, CSP, and SSP	Long and short chains, branches, polymer structures; larger frequency of WSP, CSP, and SSP chain width and length were observed in calcium and pectin methylesterase treated samples.	Zhang et al. (2019)

(*Continued*)

Table 5.1 (Continued)

Fruits and vegetables (species)	Ripening or storage	Pectin	Nanostructural properties	References
Fresh-cut honeydew melon (*Cucumis melo L. var* inodorus)	Chitosan combined with calcium chloride treatment	SSP	Short and long chain, linear single fraction, branched, multiple branched chain, cleavage point, and aggregates structures; widths: untreated, 51–60 nm (44%); day 13, mainly in 21–30 nm; lengths: untreated, 401–500 nm (33%); day 13, 301–400 nm for treated samples.	Chong, Lai, and Yang (2015)
Grapes ("Kyoho," *Vitis vinifera x V. labrusca*)	Vacuum impregnation combined with calcium lactate	WSP, CSP, and SSP	Long chains, linear single fractions, polymers, short chains, branched, releasing point, and cleavage points structures; widths: mainly within 40–60 nm; heights: CSP, 0.4–3.5 nm.	Mao et al. (2017)
Fresh-cut papayas ("Sekaki")	Vacuum impregnation with calcium lactate and pectin methylesterase (PME) treatment	CSP	Linear single fractions, polymers, branched, and conglomerate structures; the percentage of chain widths greater than 45 nm had increased 35.0% in fresh-cut papayas vacuum impregnated with calcium lactate and PME at the end of storage.	Yang, Wu, Ng, and Wang (2017)

CSP, Chelate-soluble pectin; *SSP*, sodium carbonate-soluble pectin; *WSP*, water-soluble pectin.

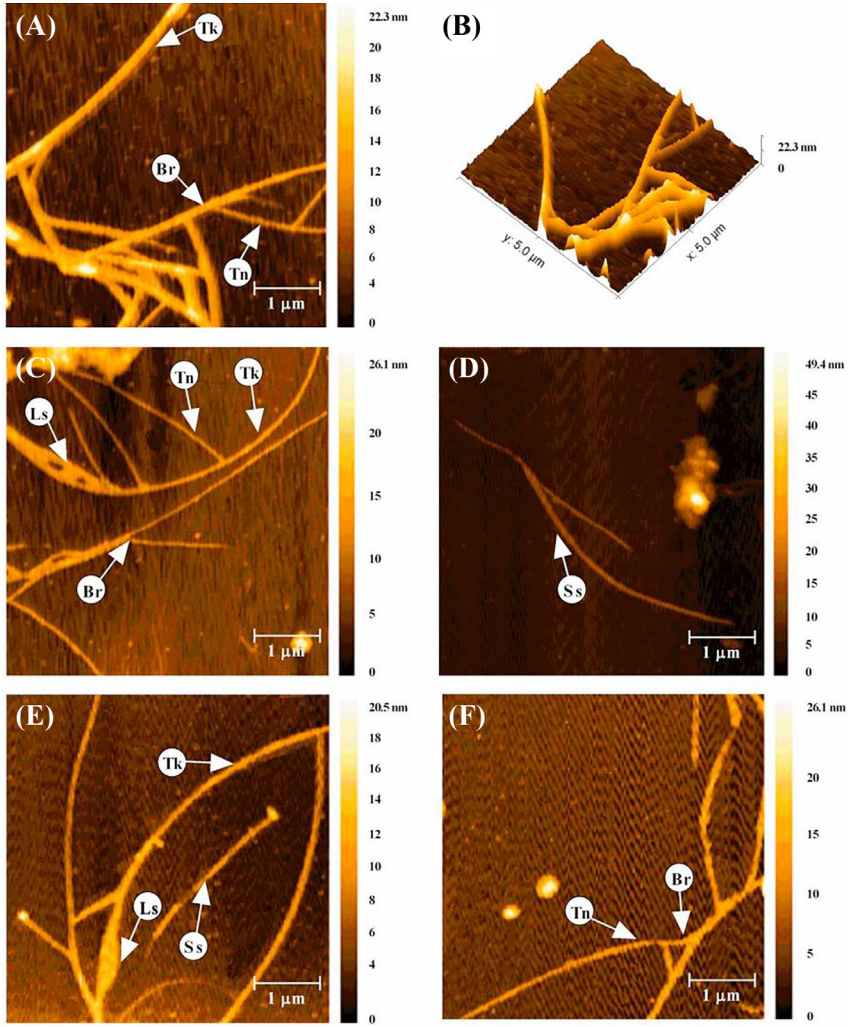

Figure 5.3 Atomic force microscopy images of sodium carbonate-soluble pectin chains in mung bean sprouts. Note: (A): control group before treatment; b: three-dimensional image of the control group before treatment; (C, D): control group at day 3; (E, F): ATP treatment group at day 3. *Br*, branched chain; *Tk*, thick chain; *Tn*, thin chain; *Ls*, loose structure; *Ss*, short straight chain. *From Chen, L., Zhou, Y., He, Z., Liu, Q., Lai, S. & Yang, H. (2018). Effect of exogenous ATP on the postharvest properties and pectin degradation of mung bean sprouts (Vigna radiata).* Food Chemistry, 251, *9–17. https://doi.org/10.1016/j.foodchem.2018.01.061*.

chain widths of ripe jujubes were less than 40 nm (Wang et al., 2012). The widths and lengths of CSP of apricot were larger than that of fruits treated with 1% $CaCl_2$. The treated group maintained larger quantitative parameters of CSP, and this was probably due to the ionic cross-linking

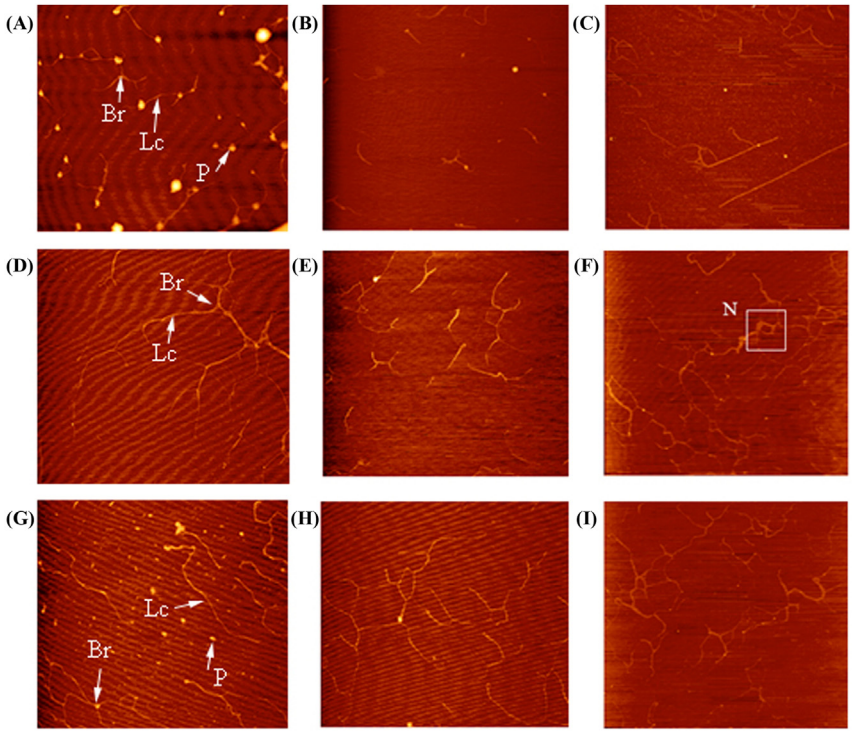

Figure 5.4 Atomic force microscopy images of water-soluble pectin (images A–C), chelate-soluble pectin (images D–F), and sodium carbonate-soluble pectin (images G–I) chains in cherry tomatoes. Note: A, D, G, images from cherry tomatoes of fresh fruit; B, E, H, images from cherry tomatoes of the calcium lactate treated group (15 min, and 15°C); C, F, I, images from cherry tomatoes of the ultrasound combined with calcium lactate treated group (20 W/L, 15 min, and 15°C); Scan area, 5.000 × 5.000 μm. *Lc*, Long straight chains; *Sc*, short chains; *Br*, branched chains; *P*, polymer structure; *N*, net-like structure. *From Zhang, L., Wang, P., Sun, X., Chen, F., Lai, S. & Yang, H. (2020). Calcium permeation property and firmness change of cherry tomatoes under ultrasound combined with calcium lactate treatment.* Ultrasonics Sonochemistry, *60, 104784. https://doi.org/10.1016/j.ultsonch.2019.104784.*

of HG s through calcium among pectin molecules. Meanwhile, the high calcium content in the cell wall could induce an increase in the cross-linking ability of HG s (Liu et al., 2009). The widths and lengths of pectin chain in berry fruits (strawberries, tomatoes, and Chinese red bayberry) were roughly equivalent to that of stone fruits (Chen et al., 2011; Li et al., 2018; Xin et al., 2010).

Pectin is in the middle lamella of plant tissues, and is the major component of cell wall. It may undergo structural changes during fruit

ripening, storage, and process. This resulted in decreasing firmness and facilitated infestation by pathogens. Therefore postharvest fruit decay increased and the quality of fresh fruits decreased (Lin et al., 2010). AFM has been extensively used to observe differences of pectin structures with different cultivars, ripening stage, and storage of peach (Zhang et al., 2012), jujubes (Wang et al., 2012), apricot (Liu et al., 2009), tomatoes (Xin et al., 2010), and Chinese cherry (Zhang et al., 2008). Liu et al. (2009) found that the firmness changed along with the changes in morphology of pectin molecules for apricot during storage (Liu et al., 2009). During the ripening, the widths of pectin chains of tomatoes decreased and a large of pectin polymers degraded with the decreased firmness (Xin et al., 2010). Zhang et al. (2010) observed that there was a relationship between the width of SSP chains of peaches and its firmness (Zhang et al., 2010). The self-assembled network of pectin in cell walls of carrots of different ripening stages was observed, and the results indicated that the network decomposed into individual molecules led to the softening of fruits and vegetables (Cybulska, Zdunek, & Kozioł, 2015).

In recent years, the extracellular materials impregnation in fruit and vegetables attracted great interest. Extracellular materials have a close relationship with fruit pectin. Preservation effects could be observed according to the AFM results, for example, AFM was used to observe the nanostructure of SSP of postharvest fresh-cut honeydew melon coated by calcium chloride, chitosan, and their combination, and these results indicated that there was a close relationship between the firmness and the nanostructure of SSP in fresh-cut honeydew melon. Meanwhile, the short and narrow SSP chains corresponded to less firmness (Chong et al., 2015). In addition, extracellular ATP could activate a specific recognition mechanism, and this could elevate the content of cytosolic free calcium ions (Ca^{2+}). AFM images were used to observe effects of exogenous ATP on the degradation of pectin in mung bean sprouts (*Vigna radiata*), and the results indicated that the treatment of ATP could slow the degradation of pectin. Meanwhile, pectin backbone width (47.1%) and height were higher than the control (45.6%) (Chen et al., 2018).

As one of the impregnation solutions, calcium could enhance fruit cell walls. It could keep the functional and structural integrity of membranes through the formation of cross-links or bridges with uronic acid carboxyls (Tappi et al., 2016). During the processing and storage of fruit, calcium that existed in cell walls could prevent tissue softening. Calcium cross-linked with pectin chains plays an important role in maintaining the

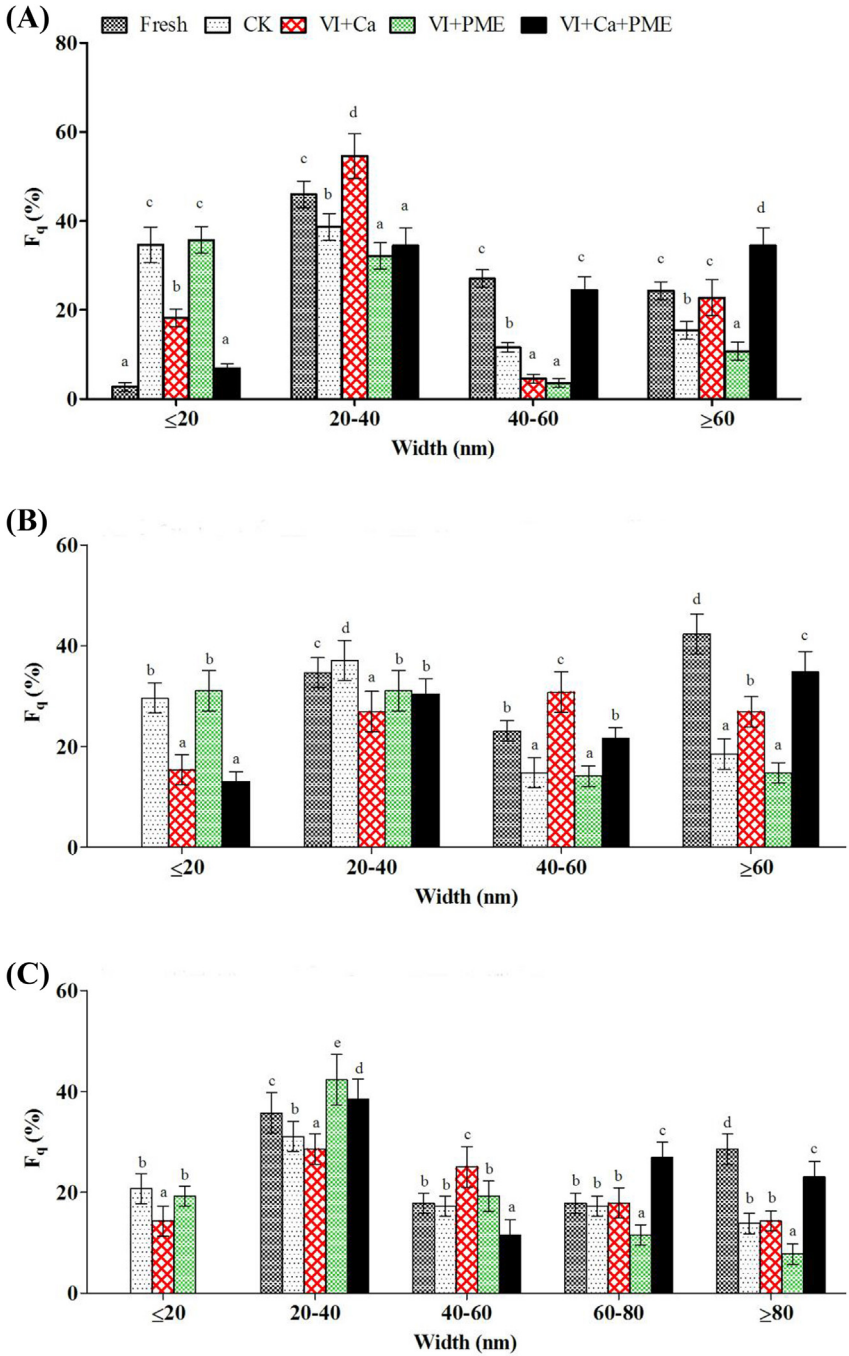

Figure 5.5 Width of (A) water-soluble pectin, (B) chelate-soluble pectin, and (C) sodium carbonate-soluble pectin chains in jujubes. Note: Fresh, untreated fresh jujubes (0 day); CK, jujubes treated with vacuum impregnation (VI) with an isotonic

texture of fruit (Chen et al., 2011; Lai et al., 2013; Liu et al., 2017). The enhancement of calcium ions into the tissue of raw materials could improve the texture and limit softening (Radziejewska-Kubzdela, Biegańska-Marecik, & Kidoń, 2014). Thus, different types of physical technology combined with impregnation solutions were used to prevent fruit decay and maintain their quality.

Vacuum impregnation (VI) and ultrasound could efficiently enhance external solutions in the tissues of vegetable and fruit to improve their physicochemical, sensory, and nutritional properties (Radziejewska-Kubzdela et al., 2014; Yusof, Wadsö, Rasmusson, & Gómez Galindo, 2017; Zhi et al., 2017). The internal gas and external solution change during the VI process of porous products. Ultrasound could enhance the penetration of compounds from extracellular to intracellular environment. What's more, the firmness of fruit was affected by the intense pressure generated during the cavitation process of ultrasound (Duarte et al., 2018).

Effects of VI on the nanostructures of CSP and SSP were investigated by AFM, and the results showed that calcium inhibited CSP and SSP degraded into short branches during the VI process (Mao et al., 2017). Li et al. studied the nanostructure properties of CSP of VI-treated Chinese red bayberries, and the results showed that CSP had large widths and lengths in calcium ascorbate impregnated group. Meanwhile, vacuum impregnated with 2% calcium ascorbate could prevent the dissociation and degradation of CSP (Li et al., 2018). Zhang et al. observed effects of pectin methylesterase (PME) and calcium chloride on the quality of jujubes under VI, and the frequencies of molecules in WSP, CSP, and SSP with a width ≥ 60 nm were the highest in the VI + Ca + PME group at the end of storage. VI + Ca + PME treatment could delay the degradation of CSP, WSP, and SSP (Fig. 5.5) (Zhang et al., 2019). The

◀ sucrose solution (56 days); VI + Ca, jujubes treated with vacuum impregnation (VI) combined with calcium chloride (56 days); VI + PME, jujubes treated with vacuum impregnation (VI) with an isotonic sucrose solution (56 days); VI + Ca, jujubes treated with vacuum impregnation (VI) combined with calcium chloride (56 days); VI + PME, jujubes treated with VI combined with pectin methylesterase (56 days); VI + Ca + PME, jujubes treated with VI combined with calcium chloride and pectin methylesterase (56 days); *Fq*, the percentage of pectin chains of particular width among all the chains observed. Error bars represent the standard deviation of the mean of three replicates. Different small case letters indicate a significant difference at $P < .05$ among different treatment methods. *From Zhang, L., Wang, P., Chen, F., Lai, S., Yu, H., & Yang, H. (2019). Effects of calcium and pectin methylesterase on quality attributes and pectin morphology of jujube fruit under vacuum impregnation during storage.* Food Chemistry, 289, *40–48. https://doi.org/10.1016/j.foodchem.2019.03.008.*

proportion of chain widths greater than 45 nm increased 35.0% in fresh-cut papayas at the end of storage, which were impregnated with calcium lactate and PME (Yang et al., 2017). Zhang et al. also used ultrasound to increase the permeation of calcium, and investigated the effects of ultrasound on the nanostructure of pectin in strawberries and cherry tomatoes. The results indicated that the percentage of width ≥ 90 nm and length ≥ 800 nm CSP molecules was larger for strawberries treated by the combination of ultrasound and calcium. A similar phenomenon of CSP and SSP was observed in cherry tomatoes (Zhang et al., 2020; Zhang, Zhao, Lai, Chen, & Yang, 2018).

The edible coating used to prolong the shelf life of vegetables and fruits attracted great attention, especially for the biodegradable and environment-friendly materials. The main ingredients of edible coatings are polysaccharides, proteins, and lipids. Chitosan, protein, and their complexes have been used to preserve fruits and vegetables for their biodegradability, biocompatibility, nontoxicity, and antimicrobial activity. Effects of edible coating on the shelf life and cell wall polysaccharides of vegetables and fruits were investigated by AFM. Zhang et al. (2018) found that the SPI-chitosan coating could inhibit the degradation of pectin. F_q (the percentage of particular length or width of pectin chains among all chains investigated by AFM) of widths ≥ 61 nm and lengths ≥ 3 μm of pectin molecules was larger in samples coated by SPI-chitosan (Zhang, Chen, Lai, Wang, & Yang, 2018). Xin, Jin, Chen, Lai, and Yang (2020) reported that more linked, branched, and long SSP chains existed in chitosan-coated sweet cherries. Widths of the pectin backbone in sweet cherries also could be maintained by chitosan coating (Xin et al., 2020). Meanwhile, the structural analysis by AFM showed that CSP degradation could be inhibited when coated by rice bran wax, the width of CSP molecules was in the range of 15−250 nm, and their vertical heights varied from 0.2 to 2.0 nm. Compared to the control, higher frequency (F_q) of CSP molecules with large widths and lengths were observed in waxed fruits (Zhang et al., 2017).

Cell wall stiffness is important to elucidate the mechanism of fruit softening, and cell walls become loosen and weaker during fruit ripening. Meanwhile, it is difficult to measure the cell wall elastic properties at micrometer scale. AFM can image the surface morphology of nanometer resolution and sense the nanomechanical properties. Thereby, AFM has been used to analyze the mechanical properties of plant cells. Changes in cell wall stiffness during pear ripening could be evaluated by AFM, which

could be used to investigate the cell wall components affecting cell wall mechanics, including neutral sugars, hemicelluloses, and related enzymes (Zdunek et al., 2016). Yang et al. used AMF to analyze the root mean square roughness (R_q) and arithmetic roughness (R_a) of "Jinxiu" yellow peach skin (*Prunus persicu* L. *Batsch.*) during storage. The R_a and R_q increased for both the controlled atmosphere (CA) and regular air (RA) group, while the values of CA group were smaller than that of RA group. AFM also could observe the three-dimensional profiles of the skin (Fig. 5.6) (Yang, An, Feng, & Li, 2005).

Pieczywek et al. investigated the cell wall stiffness of ultrasonically (US) treated apple by AFM. There was a significant linear decrease in cell wall stiffness along with the US treatment time. US caused the pronounced disassembly of the polysaccharide network according to AFM results (Pieczywek, Kozioł, Konopacka, Cybulska, & Zdunek, 2017). The nanomechanical properties of fruit cells observed could provide insights on the internal fruit properties and the changes of these properties over time, which affected the quality of fruits. Cárdenas-Pérez et al. obtained Young's modulus (YM) of apple tissue at cellular level using AFM. Meanwhile, the relationship between apple tissue and other macroscopic physical parameters was utilized to evaluate the ripeness during the storage of apples (Cárdenas-Pérez et al., 2017).

5.2.2.2 Nanostructural analysis of pectin

AFM is a valuable tool to investigate the nanostructure and nanomechanical properties of single biomolecules and assemblies, including pectin, and is appropriate to observe single molecules on a nanometer scale. It needs minimal sample and simple preparation, and can distinguish overlapping molecules from true branching points through the height analysis. For example, peanut polysaccharide molecules exhibited interweaved or overlapped chains morphology (Ye et al., 2020). The length of molecules with a curved shape was difficult to estimate (Cybulska et al., 2015).

Researchers used AFM to investigate structures of pectin in an aqueous solution. Compared to high methoxyl pectin, low methoxyl pectin networks couldn't be dissociated when dissolved in water with concentrations less than 6.6 μg/mL (Fishman et al., 2015). Pea soluble polysaccharides possessed star-like structures with side chains according to the AFM images (Cheng et al., 2018). Guo et al. investigated the nanostructure of copper-precipitated pectin and copper-unprecipitated pectin from sugar beet by AFM. Pectin precipitated by copper had branched fibrous

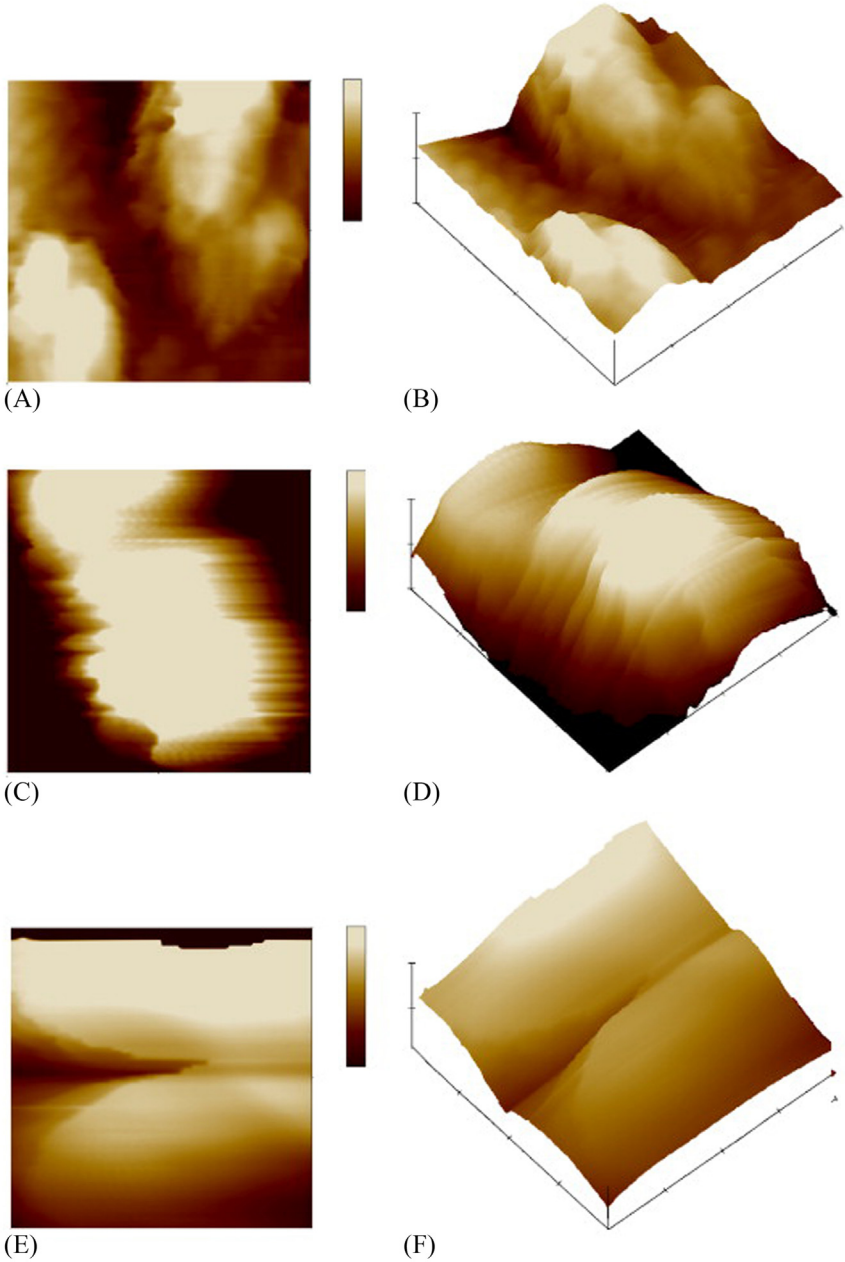

Figure 5.6 Profiles of peach skin at different stage of controlled atmosphere storage by atomic force microscopy. Note: (A) and (B) plane and three-dimensional profiles after 15-day storage, respectively. Scan area = 2.003 mm, height bar = 50 nm. (C) and (D) plane and three-dimensional profiles after 30-day storage respectively. Scan

structures, while pectin unprecipitated by copper exhibited distinguishable granular-like shapes (Guo, Meng, Zhu, Zhang, & Yu, 2015).

Branched morphology and self-assembly properties of pectin also could be investigated by AFM. Branched-chain morphology of RG I enriched pectin of mandarin citrus peel was observed by AFM (Zhang et al., 2018). The percentage content of branched RG I of chelator-extractable pectin, water-soluble pectin, and sodium carbonate extractable pectin from black tomato pomace were 5.32%, 10.97%, and 29.08%, respectively (Zhang et al., 2020).

The AFM images revealed that sodium carbonate molecules from apple fruit structurally resembled rod-like objects, which consisted of relatively long linear sections separated by bend points or branches (Pieczywek, Kozioł, Płaziński, Cybulska, & Zdunek, 2020). AFM revealed the self-assembly of high- and low-methoxyl pectin of different concentrations. Pectin would link and aggregate with the raise of concentration. Lengths of high- and low-methoxyl pectin of 0.005 mg/mL were from 19.22 to 312.11 nm. AFM enabled research works on the model of "egg-box" of pectin-calcium ions from a new perspective (Wang, Fei, Wang, Zan, & Zhu, 2020). The morphology of ultrahigh methoxylated pectin aggregation presented a network structure and irregular clusters at 10 and 1 μg/mL based on AFM (Liu et al., 2020). AFM research works indicated the self-organize on mica of chicory root pectin extracted by citric acid (CEP). These revealed that the random coil conformation was caused by the interaction of multiple branching. However, chicory root pectin extracted by alkaline (AEP) showed long linear filamentous structures (Zhang et al., 2020).

AFM could investigate the single-molecular behavior under applied force, and provide important kinetic parameters of pectin single-molecular (Zlatanova & van Holde, 2006). Cybulska et al. used AFM to stretch the galacturonic acid oligomers, and defined their mechanical properties (Cybulska, Brzyska, Zdunek, & Woliński, 2014).

◀ area = 2.000 mm * 2.000 mm, height bar = 50 nm. (C) and (D) plane and three-dimensional profiles after 30-day storage respectively. Scan area = 2.000 mm * 2.000 mm, height bar = 100 nm. (E), (F) plane and three-dimensional profiles after 45-day storage, respectively. Scan area = 2.004 mm * 2.004 mm, height bar = 100 nm. *From Yang, H., An, H., Feng, G., & Li, Y. (2005). Visualization and quantitative roughness analysis of peach skin by atomic force microscopy under storage.* LWT – Food Science and Technology, 38*(6), 571–577. https://doi.org/10.1016/j.lwt.2004.09.007*.

5.2.3 Cellulose

As an important biopolymer and the most abundant renewable resource, cellulose is widely applied due to its biocompatibility, availability, biodegradability, and sustainable production potential (Khorasani & Shojaosadati, 2017). Cellulose is composed of long chains with unbranched β (1→4) linked D-glucopyranosyl units, while the lengths of β (1→4) linked D-glucan rely on the species, maturity, and growth environment of the plant (Venkateshaiah et al., 2020). It usually contains 500−7500 D-glucose monomers.

Cellulose is the basic structural molecule of plant cell walls, and its structural arrangements affect the functional properties of fruits and vegetables. The relationship among cellulose microfibrils properties, diameter, crystallinity, and texture of fruits was investigated. Cybulska et al. reported that microfibrils of lower crystallinity of crisp apple cultivars were thicker than that of softer apple cultivars (Cybulska, Zdunek, Psonka-Antonczyk, & Stokke, 2013). However, cellulose microfibrils had similar diameters in different pear cultivars (Zdunek et al., 2016).

AFM could be used to evaluate the morphology and quantity parameter (diameter) of cellulose microfibrils. Liu et al., 2017 investigated the nanostructure of carboxymethylated polysaccharide (CMSERP) by AFM, and the results revealed that CMSERP could be dispersed in 0.05 M sodium sulfate and aggregated in water (Liu et al., 2017). The morphology of a coprocessed bio-based polymer observed by AFM showed that the polymers exhibited almost oval and spherical particles, and the surface of the particles had a loosely packed structure and was composed of irregular, globular structural elements (Singh, Nwabor, Ontong, Kaewnopparat, & Voravuthikunchai, 2020). Cheikh Rouhou, Abdelmoumen, Thomas, Attia, and Ghorbel (2018) reported that diameter of cactus rackets dietary fibers was 80 nm (Cheikh Rouhou et al., 2018). The diameter of cellulose from apple pomace, carrot pomace, tomato pomace, and cucumber pomace were analyzed by AFM, and the results showed that the distribution of microfibrils was similar. Furthermore, the largest diameter fraction was from 20 to 30 nm, while the average thickness of cellulose microfibrils from four pomaces varied (carrot pomace: 28.68 (± 9.27) nm; cucumber pomace: 29.03 (± 9.43) nm; apple pomace: 28.73 (± 10.17) nm; and tomato pomace: 32.24 (± 10.35) nm) (Szymańska-Chargot, Chylińska, Gdula, Kozioł, & Zdunek, 2017). The diameters of cellulose microfibrils of onion and maize were 3−4 nm according to AFM analysis (Ding et al., 2012; Zhang, Zheng, & Cosgrove, 2016). Meanwhile, the diameter of ultrathin microfibril was 1−2 nm in peach and strawberry fruits (Niimura, Yokoyama, Kimura, Matsumoto, & Kuga, 2010).

AFM could efficiently evaluate the width, length, and aspect ratios of cellulose nanocrystal (Nagalakshmaiah, kissi, Mortha, & Dufresne, 2016).

5.2.4 Others

AFM could be used to observe the conformation of individual macromolecule, and analyze the quantitative parameters of xanthan. In pure water, xanthan existed a single helix structure, while double helix conformation was observed in KCl solution. The length of xanthan decreased from 1651 to 450 nm, and its number-average contour length decreased from 417 to about 150 nm (Camesano & Wilkinson, 2001; Yang & Zhang, 2009). Xanthan from different sources had different structural features according to AFM results. For example, xanthan of the wild-type strain *Xanthomonas campestris* B100 had branching and overlapping structures, while that of the strain JBL007 had no branching. The xanthan of acetate-free had single- and double-stranded areas with no branching, while xanthan of pyruvate-free had a branched and homogenous structure with single and double strands (Teckentrup et al., 2017; Venkateshaiah et al., 2020).

The nanostructure and self-assembly of XG in plants were observed by AFM. The mean height and mean length of was 2.3 ± 0.5 nm and 640 ± 360 nm, respectively. XG chains had a helical structure and could be aggregated as cross-like and a parallel-like assembly (Kozioł, Cybulska, Pieczywek, & Zdunek, 2015).

Polysaccharide hyaluronan (HA) exists in the extracellular, pericellular, and intracellular matrix. It consists of repeated disaccharide structure poly [(1/3)-b-DGlcNAc-(1/4)-b-D-GlcA-]. The conformations and specific binding interactions of HA have a close relationship to its biological functions. AFM could provide an alternative view of the conformation of HA with different sample preparation. An extended conformation could be observed when HA deposited on a prehydrated mica surface. However, HA favored relaxed, weakly helical, and coiled conformations when it was deposited on freshly cleaved mica. Necklace forms, thick rods, networks, and twisted fibers were also observed in intramolecularly condensed and intermolecular association of HA (Cowman et al., 2005).

Li et al. (2017) investigated the chain conformation of four sulfated polysaccharides from sea cucumbers by AFM. The chain conformation of fucosylated chondroitin sulfate (fCS) from *Isostichopus badiono-tus* (fCS-Ib), fCS derived from *Pearsonothuria graeffei* (fCS-Pg), and fucoidan from fuc-Pg were random coil with polysaccharide chain outstretched, while fucoidan from fuc-Ib was spherical conformation in solution. fuc-Pg and fuc-Ib were linear polysaccharides without side branches, while fucose was the only monosaccharide. The lengths

of fCS-Pg, fCS-Ib, and fuc-Pg chain were from 100 to 1000 nm. Meanwhile, molecular aggregation took place among polysaccharide chains. Fuc-Ib formed a sphere with a diameter of about 100 nm, and had no linear chains on the surface of mica. Chain conformation could be used to determine the hypolipidemic activity of sulfated polysaccharides with regular structure (Li et al., 2017).

Lots of polysaccharides from seaweeds are hydrocolloids, and could be utilized to adjust rheological properties of food systems. *Eucheuma* is the red seaweed found in Southeast Asia. Yang et al. (2020) investigated the effect of extraction temperature on structures of extracted polysaccharides from *Eucheuma*. According to AFM results, the heights of polysaccharides decreased along with the increase in temperature. Polysaccharides of side-by-side association tended to be formed under relatively low temperature (Fig. 5.7) (Yang & Yang, 2020). Other polysaccharides such as κ-carrageenan (KC) and chitosan also could be observed by AFM. An interconnected porous fibrous network was observed in KC (Sow, Nicole Chong, Liao, & Yang, 2018). Yang and Yang (2020) also found that side-by-side association was observed in KC with lower temperatures extraction. The contour lengths and average height of single chitosan strands were 94−178 nm and 0.45 ± 0.04 nm, respectively (Kocun, Grandbois, & Cuccia, 2011).

AFM data of nanostructural characters of polysaccharides are shown in Table 5.2.

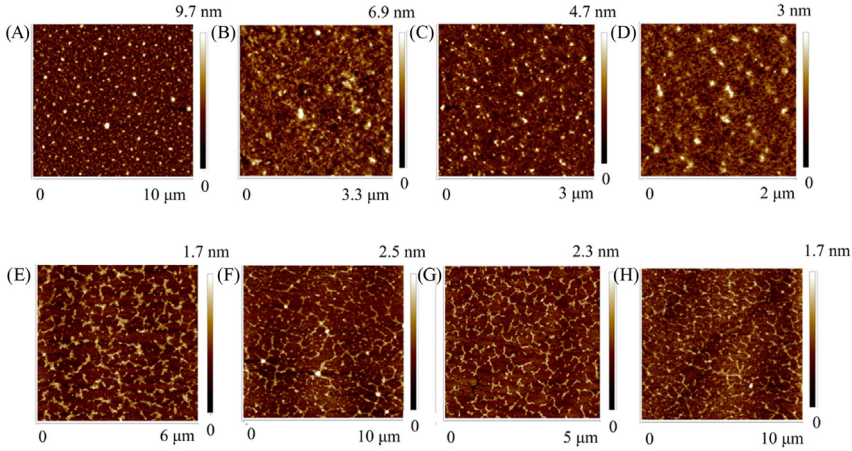

Figure 5.7 Atomic force microscopy images of different extracts. AFM images of: (A) 0.02 mg/mL 60°C extract; (B) 0.02 mg/mL 70°C extract; (C) 0.02 mg/mL 80°C extract; (D) 0.02 mg/mL 90°C extract; (E) 0.002 mg/mL 60°C extract; (F) 0.002 mg/mL 70°C; (G) 0.002 mg/mL 80°C extract; (H) 0.002 mg/mL 90°C *From Yang, D. & Yang, H. (2020). The temperature dependent extraction of polysaccharides from eucheuma and the rheological synergistic effect in their mixtures with kappa carrageenan.* LWT – Food Science and Technology, 129, *109515. https://doi.org/10.1016/j.lwt.2020.109515*.

Table 5.2 Atomic force microscopy data of nanostructural characters of polysaccharides.

Polysaccharides	Sources	Nanostructural properties	References
Pectin	Citrus peel	Linear strands, singly branched, multiply branched, and polymer structures.	Zhang et al. (2013); Zhang, Zhang, Liu, Ding, and Ye (2015)
	Tomato pectin	Linear and branched structures, weight average (L_W) and number average (L_N) contour lengths were 174 and 132 nm, respectively; $L_W/L_N = 1.32$.	Kirby, MacDougall, and Morris (2008)
	Sugar beet	Unaggregated molecules, and branched structures, weight average (L_W) = 138 nm, number average (L_N) = 108 nm, $L_W/L_N = 1.27$.	Kirby et al. (2008)
	Apple peel	Network structure (pH 4 and 9), aggregates (pH11); height: 0.51 ± 0.25 nm (pH 3); length: >5000 nm (pH 4 and 9); ≤ 1000 nm (pH 7 and 11).	Gawkowska, Cieśla, Zdunek, and Cybulska (2019)
Starch	Wheat	R_a and R_q vales: 14.2 ± 2.7 nm and 11.3 ± 2.3 nm for native starch; 58.2 ± 8.0 nm and 46.5 ± 7.5 nm for damaged starch.	Barrera et al. (2013)
	Potato	Rough and heterogeneous morphologies, "blocklets" structures; diameter, 10−100 nm; R_q, 4.42−10.30 nm; R_a, 3.58−8.16 nm.	(Chen et al., 2019)
	Corn	Larger column arrangements and spherical particles.	Sujka, Jamroz (2009)
Hemicellulose	Pear	Rod-like shape, tangled assemblies; length: 20−400 nm ("Conference"), and 80−400 nm ("Xenia").	(Zdunek, Kozioł, Pieczywek, & Cybulska, 2014)

(*Continued*)

Table 5.2 (Continued)

Polysaccharides	Sources	Nanostructural properties	References
Cellulose	Apple pomace, carrot pomace, tomato pomace, cucumber pomace	The average cellulose microfibril thickness: 28.68 (± 9.27) nm for carrot pomace, 29.03 (± 9.43) nm for cucumber pomace, 28.73 (± 10.17) nm for apple pomace, and 32.24 (± 10.35) nm for tomato pomace; the cellulose microfibril diameter for carrot, cucumber, and apple pomaces with the largest diameter fraction (more than 45% of estimated microfibrils) between 20–30 nm, while cellulose microfibrils isolated from tomato, the distribution maximum (more than 45% of estimated microfibrils) is shifted to the thicker fractions of 25–35 nm.	Szymańska-Chargot et al. (2017)
Chitason	–	Contour lengths, 94–178 nm; average heights, 0.45 ± 0.04 nm.	Kocun et al. (2011)
Xanthan	*Xanthomonas campestris*	Double helix conformation, aggregates.	Wang, Xiang, Li, Zhang, and Bai (2021)
Xyloglucan	Tamarind seed	Rod-like structures, mean height of 2.3 ± 0.5 nm and mean length of 640 ± 360 nm; helical structure with a period of 115.8 ± 29.2 nm.	Kozioł et al. (2015)
Fucosylated chondroitin sulfate	*Pearsonothuria graeffei* (fCS-Pg), *Isostichopus badionotus* (fCS-Ib)	fCS-Pg, fCS-Ib, random linear chains with a few spherical aggregations; lengths, 100–1000 nm.	Li et al. (2017)
κ-carrageenan	SeaKem CM 611	Interconnected porous fibrous network	Sow et al. (2018)
Eucheuma polysaccharide	*Eucheuma*	side-by-side association	Yang and Yang (2020)
Peanut polysaccharide	Peanut	spheres; diameter, 15–50 nm; lengths, 100–300 nm.	Ye et al. (2020)

Note: R_a, roughness average; R_q, root mean square roughness.

5.3 Measurement of molecule interactions of polysaccharides and food components

Components could interact with each other and form complexes in food systems. For example, there are complex interactions among polysaccharides, proteins, lipids, and their modified products. Research on a single component is usually insufficient to understand the food framework. Thereby, research on interaction among components is needed. AFM could be applied to investigate the real structure of complexes of natural materials. Intra- and intermolecular interaction forces (50 pN to 1−2 nN) could be investigated by AFM (Zlatanova & Leuba, 2002).

5.3.1 Polysaccharides-polysaccharides

Nowadays, pectin is used as a biopolymer-based food packaging for its low cost and good film-forming property. However, the edible films prepared using pure pectin have a poor barrier, thermo mechanical, and water resistance properties. Crystalline nanocellulose (CNC) could strengthen the barrier and mechanical properties of final films. Thus, using nanoreinforcement of biopolymers to produce bionanocomposites attracted great interest. AFM images could provide the morphology and distribution of CNC in pectin-CNC composite films. CNC particles were dispersed uniformly on the surface of the pectin-CNC (2% and 5%) composite films without any aggregation. The presence of uneven plateaus on the AFM images increased with the increase of CNC level, and this was due to the agglomeration of CNC (Chaichi, Hashemi, Badii, & Mohammadi, 2017). Chaichi et al. reported that nanocellulose could enhance the properties of pectin films based on the structure and properties of films determined by AFM (Chaichi et al., 2017).

AFM also could be used to evaluate the effect of noncellulosic polysaccharides on the structure and arrangement of cellulose microfibrils (Szymańska-Chargot et al., 2017). Hiasa et al. investigated the effects of pectin on the aggregation of cellulose nanofibers (CNFs) by AFM. AFM images showed that the pectin covered the surfaces of the CNFs, and the CNFs obtained from mandarin peel were finer than those obtained from wood cellulose (Hiasa, Kumagai, Endo, & Edashige, 2016).

The surface morphology of the entrapment biocomposite (pectin-nonstarch nanofibers) was analyzed in the air at ambient temperature, using the contact mode of AFM. The nanofibers were intercalated into a pectin matrix. A percolating NC (nanofibers of chitin) network developed

within the pec-NC biocomposite according to the uniform morphology and a homogenous distribution of the nanofibrillar network structure. The surface of the biocomposite was continuous without pores and cracks (Khorasani & Shojaosadati, 2017).

5.3.2 Polysaccharides-protein

The multilayer microcapsules prepared by high methoxyl pectin and soy protein isolate fibrils were determined by AFM, and the results showed that the thickness of the soy protein isolate fibrils varied from 1 to 10 nm, and their structures were highly branched (Ansarifar, Mohebbi, Shahidi, Koocheki, & Ramezanian, 2017).

Pectin and MTGase could be used to improve the rheological behavior, gel, and thermal properties of fish scales gelatin. According to the results of AFM and scanning electron microscopy analysis, MTGase catalyzed the cross-links among soluble fish scales gelatin-pectin complexes, which affected the increase of gel strength, rheological behavior, and melting temperature of modified complex gels (Huang et al., 2017).

AFM images confirmed the spherical morphology and nanostructure of WPC-pectin complexes (Ghasemi, Jafari, Assadpour, & Khomeiri, 2017). A compact conformation of sugar beet pectin was observed to be covalently bridged with the amino groups of lysine residues of the proteinaceous moiety according to AFM analysis (Lin, Yu, Ai, Zhang, & Guo, 2020). Structural characteristics of ploysaccharide-protein-based films, such as gelatin−pectin, fish gelatin/chitosan nanoparticle composites, hydroxypropyl methyl cellulose and zein nanoparticles, were also elucidated by AFM (Farris et al., 2011; Gilbert, Cheng, & Jones, 2018; Hosseini, Rezaei, Zandi, & Farahmandghavi, 2016).

Sow et al. (2018) evaluated the effect of the ratio of fish gelatin (FG) and KC on the interaction and structures of FG using AFM. With low amount of KC in FG, a few spherical and irregular aggregates were observed in FG. Complex coacervates were obvious with KC: FG of 2:98 and 4:96, while the bicontinuous structure was found when KC: FG was 10:90. Dense complex coacervates regions were also found with KC: FG at 10:90 (Fig. 5.8). The morphology of the tea water-insoluble protein/KC (TWIP/KC) mixtures was also assessed by AFM. The results illustrated the aggregation behavior of TWIP. The protein particles progressively clustered with the increase of KC addition (Ren et al., 2021).

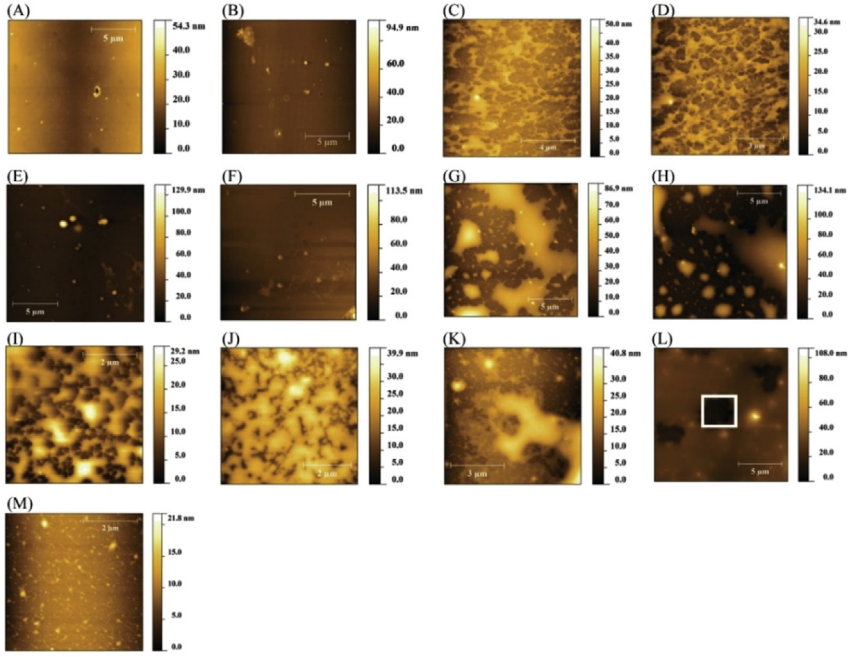

Figure 5.8 Nanostructure. Note: (A, B) fish gelatin (FG); (C, D) κ-carrageenan (KC); and the FG-KC mixtures at different mixing ratios (KC:FG, w/w) of (E, F) 0.5:99.5 (FGC1); (G, H) 2:98 (FGC3) and (I, J) 4: 96 (FGC4); (K, L, M) 10:90 (FGC6) featuring bicontinuous phase comprising (K, L) a complex coacervates region and (M) thin fibril structure underneath the dense region (white square) of (M). *The images were obtained from samples prepared at 0.01% (w/v) of KC-FG mixture. *From Sow, L. C., Nicole Chong, J. M., Liao, Q. X., & Yang, H. (2018). Effects of κ-carrageenan on the structure and rheological properties of fish gelatin.* Journal of Food Engineering, 239, *92–103. https://doi.org/10.1016/j.jfoodeng.2018.05.035*.

5.4 Conclusions

AFM opened new horizons in imaging and force measurements of food polysaccharides. In this chapter, the applications of AFM in starch, pectin, cellulose, and other polysaccharides were discussed. AFM could provide the surface morphology, roughness parameters, internal structures of starch granules, and reveal the surface properties of starch films. Furthermore, AFM could be utilized to investigate morphology, qualitative, and quantitative characteristic of pectin, cellulose, and other polysaccharide molecules. AFM also could be used to observe the three-dimensional structure of pectin molecules, and stretch single pectin molecular chains. This

chapter was focused on introducing structure changes of pectin molecules of fruits and vegetables during storage by AFM. These observations could provide novel ideas for fruits and vegetables preservation. Moreover, AFM was significantly contributed to understand the intra and intermolecular interactions, which played a key role in understanding the food framework. AFM could provide more opportunities to improve food quality during processing and preservation.

Acknowledgment

This study was funded by the Young-aged Backbone Teacher Funds of Henan Province of China (2020GGJS083), Applied Basic Research Project (Agricultural) Suzhou Science and Technology Planning Programme (SNG2020061), Natural Science Foundation of Jiangsu Province (BK20181184), Singapore Ministry of Education Academic Research Fund Tier 1 (R-160−000-A40−114), and an industry grant supported by Shenzhen Zhiyun Optoelectronics Co., Ltd. (R-143−000-A24−597).

Declaration of competing interest

We declare that there was no commercial or associative interest that represents a conflict of interest in connection with this manuscript. We have no financial and personal relationships with other people or organizations that can inappropriately influence our work.

References

Aguilar-Sánchez, R., Munguía-Pérez, R., Reyes-Jurado, F., Navarro-Cruz, A. R., Cid-Pérez, T. S., Hernández-Carranza, P., … Avila-Sosa, R. (2019). Structural, physical, and antifungal characterization of starch edible films added with nanocomposites and Mexican Oregano (Lippia berlandieri Schauer) essential oil. *Molecules (Basel, Switzerland)*, *24*(12), 2340. Available from https://doi.org/10.3390/molecules24122340.

Ansarifar, E., Mohebbi, M., Shahidi, F., Koocheki, A., & Ramezanian, N. (2017). Novel multilayer microcapsules based on soy protein isolate fibrils and high methoxyl pectin: Production, characterization and release modeling. *International Journal of Biological Macromolecules*, *97*, 761−769. Available from https://doi.org/10.1016/j.ijbiomac.2017.01.056.

Baldwin, P. M., Davies, M. C., & Melia, C. D. (1997). Starch granule surface imaging using low-voltage scanning electron microscopy and atomic force microscopy. *International Journal of Biological Macromolecules*, *21*(1−2), 103−107. Available from https://doi.org/10.1016/S0141-8130(97)00048-2.

Barrera, G. N., Calderón-Domínguez, G., Chanona-Pérez, J., Gutiérrez-López, G. F., León, A. E., & Ribotta, P. D. (2013). Evaluation of the mechanical damage on wheat starch granules by SEM, ESEM, AFM and texture image analysis. *Carbohydrate*

Polymers, *98*(2), 1449–1457. Available from https://doi.org/10.1016/j.carbpol.2013.07.056.

Cai, X., Du, X., Zhu, G., & Cao, C. (2020). Induction effect of NaCl on the formation and stability of emulsions stabilized by carboxymethyl starch/xanthan gum combinations. *Food Hydrocolloids*, *105*, 105776. Available from https://doi.org/10.1016/j.foodhyd.2020.105776.

Camesano, T. A., & Wilkinson, K. J. (2001). Single molecule study of Xanthan conformation using atomic force microscopy. *Biomacromolecules*, *2*(4), 1184–1191. Available from https://doi.org/10.1021/bm015555g.

Chaichi, M., Hashemi, M., Badii, F., & Mohammadi, A. (2017). Preparation and characterization of a novel bionanocomposite edible film based on pectin and crystalline nanocellulose. *Carbohydrate Polymers*, *157*, 167–175. Available from https://doi.org/10.1016/j.carbpol.2016.09.062.

Chakraborty, I., Pallen, S., Shetty, Y., Roy, N., & Mazumder, N. (2020). Advanced microscopy techniques for revealing molecular structure of starch granules. *Biophysical Reviews*, *12*(1), 105–122. Available from https://doi.org/10.1007/s12551-020-00614-7.

Chandra Mohan, C., Harini, K., Karthikeyan, S., Sudharsan, K., & Sukumar, M. (2018). Effect of film constituents and different processing conditions on the properties of starch based thermoplastic films. *International Journal of Biological Macromolecules*, *120*, 2007–2016. Available from https://doi.org/10.1016/j.ijbiomac.2018.09.161.

Cheikh Rouhou, M., Abdelmoumen, S., Thomas, S., Attia, H., & Ghorbel, D. (2018). Use of green chemistry methods in the extraction of dietary fibers from cactus rackets (Opuntia ficus indica): Structural and microstructural studies. *International Journal of Biological Macromolecules*, *116*, 901–910. Available from https://doi.org/10.1016/j.ijbiomac.2018.05.090.

Chen, F., Liu, H., Yang, H., Lai, S., Cheng, X., Xin, Y., … Deng, Y. (2011). Quality attributes and cell wall properties of strawberries (Fragaria annanassa Duch.) under calcium chloride treatment. *Food Chemistry*, *126*(2), 450–459. Available from https://doi.org/10.1016/j.foodchem.2010.11.009.

Chen, L., Ma, R., Zhang, Z., Huang, M., Cai, C., Zhang, R., … Jin, Z. (2019). Comprehensive investigation and comparison of surface microstructure of fractionated potato starches. *Food Hydrocolloids*, *89*, 11–19. Available from https://doi.org/10.1016/j.foodhyd.2018.10.017.

Chen, L., Zhou, Y., He, Z., Liu, Q., Lai, S., & Yang, H. (2018). Effect of exogenous ATP on the postharvest properties and pectin degradation of mung bean sprouts (Vigna radiata). *Food Chemistry*, *251*, 9–17. Available from https://doi.org/10.1016/j.foodchem.2018.01.061.

Chen, Y., Chen, F., Lai, S., Yang, H., Liu, H., Liu, K., … Deng, Y. (2013). In vitro study of the interaction between pectinase and chelate-soluble pectin in postharvest apricot fruits. *European Food Research and Technology*, *237*(6), 987–993. Available from https://doi.org/10.1007/s00217-013-2071-1.

Cheng, M., Qi, J. R., Feng, J. L., Cao, J., Wang, J. M., & Yang, X. Q. (2018). Pea soluble polysaccharides obtained from two enzyme-assisted extraction methods and their application as acidified milk drinks stabilizers. *Food Research International*, *109*, 544–551. Available from https://doi.org/10.1016/j.foodres.2018.04.056.

Chong, J. X., Lai, S., & Yang, H. (2015). Chitosan combined with calcium chloride impacts fresh-cut honeydew melon by stabilising nanostructures of sodium-carbonate-soluble pectin. *Food Control*, *53*, 195–205. Available from https://doi.org/10.1016/j.foodcont.2014.12.035.

Cowman, M. K., Spagnoli, C., Kudasheva, D., Li, M., Dyal, A., Kanai, S., & Balazs, E. A. (2005). Extended, relaxed, and condensed conformations of hyaluronan observed by

atomic force microscopy. *Biophysical Journal*, *88*(1), 590–602. Available from https://doi.org/10.1529/biophysj.104.049361.

Cybulska, J., Brzyska, A., Zdunek, A., & Woliński, K. (2014). Simulation of force spectroscopy experiments on galacturonic acid oligomers. *PLoS One*, *9*(9). Available from https://doi.org/10.1371/journal.pone.0107896.

Cybulska, J., Zdunek, A., & Kozioł, A. (2015). The self-assembled network and physiological degradation of pectins in carrot cell walls. *Food Hydrocolloids*, *43*, 41–50. Available from https://doi.org/10.1016/j.foodhyd.2014.04.032.

Cybulska, J., Zdunek, A., Psonka-Antonczyk, K. M., & Stokke, B. T. (2013). The relation of apple texture with cell wall nanostructure studied using an atomic force microscope. *Carbohydrate Polymers*, *92*(1), 128–137. Available from https://doi.org/10.1016/j.carbpol.2012.08.103.

Cárdenas-Pérez, S., Méndez-Méndez, J. V., Chanona-Pérez, J. J., Zdunek, A., Güemes-Vera, N., Calderón-Domínguez, G., & Rodríguez-González, F. (2017). Prediction of the nanomechanical properties of apple tissue during its ripening process from its firmness, color and microstructural parameters. *Innovative Food Science and Emerging Technologies*, *39*, 79–87. Available from https://doi.org/10.1016/j.ifset.2016.11.004.

Dai, L., Zhang, J., & Cheng, F. (2019). Effects of starches from different botanical sources and modification methods on physicochemical properties of starch-based edible films. *International Journal of Biological Macromolecules*, *132*, 897–905. Available from https://doi.org/10.1016/j.ijbiomac.2019.03.197.

Ding, S. Y., Liu, Y. S., Zeng, Y., Himmel, M. E., Baker, J. O., & Bayer, E. A. (2012). How does plant cell wall nanoscale architecture correlate with enzymatic digestibility? *Science (New York, N.Y.)*, *338*(6110), 1055–1060. Available from https://doi.org/10.1126/science.1227491.

Duarte, A. L. A., do Rosário, D. K. A., Oliveira, S. B. S., de Souza, H. L. S., de Carvalho, R. V., Carneiro, J. C. S., … Bernardes, P. C. (2018). Ultrasound improves antimicrobial effect of sodium dichloroisocyanurate to reduce Salmonella Typhimurium on purple cabbage. *International Journal of Food Microbiology*, *269*, 12–18. Available from https://doi.org/10.1016/j.ijfoodmicro.2018.01.007.

Farajpour, R., Emam Djomeh, Z., Moeini, S., Tavahkolipour, H., & Safayan, S. (2020). Structural and physico-mechanical properties of potato starch-olive oil edible films reinforced with zein nanoparticles. *International Journal of Biological Macromolecules*, *149*, 941–950. Available from https://doi.org/10.1016/j.ijbiomac.2020.01.175.

Farris, S., Schaich, K. M., Liu, L. S., Cooke, P. H., Piergiovanni, L., & Yam, K. L. (2011). Gelatin-pectin composite films from polyion-complex hydrogels. *Food Hydrocolloids*, *25*(1), 61–70. Available from https://doi.org/10.1016/j.foodhyd.2010.05.006.

Fishman, M. L., Chau, H. K., Qi, P. X., Hotchkiss, A. T., Garcia, R. A., & Cooke, P. H. (2015). Characterization of the global structure of low methoxyl pectin in solution. *Food Hydrocolloids*, *46*, 153–159. Available from https://doi.org/10.1016/j.foodhyd.2014.12.021.

Funami, T. (2010). Atomic force microscopy imaging of food polysaccharides. *Food Science and Technology Research*, *16*(1), 1–12. Available from https://doi.org/10.3136/fstr.16.1.

Gao, W., Wu, W., Liu, P., Hou, H., Li, X., & Cui, B. (2020). Preparation and evaluation of hydrophobic biodegradable films made from corn/octenylsuccinated starch incorporated with different concentrations of soybean oil. *International Journal of Biological Macromolecules*, *142*, 376–383. Available from https://doi.org/10.1016/j.ijbiomac.2019.09.108.

Gawkowska, D., Cieśla, J., Zdunek, A., & Cybulska, J. (2019). Cross-linking of diluted alkali-soluble pectin from apple (Malus domestica fruit) in different acid-base

conditions. *Food Hydrocolloids*, *92*, 285–292. Available from https://doi.org/10.1016/j.foodhyd.2019.02.010.

Ghasemi, S., Jafari, S. M., Assadpour, E., & Khomeiri, M. (2017). Production of pectin-whey protein nano-complexes as carriers of orange peel oil. *Carbohydrate Polymers*, *177*, 369–377. Available from https://doi.org/10.1016/j.carbpol.2017.09.009.

Gilbert, J., Cheng, C. J., & Jones, O. G. (2018). Vapor barrier properties and mechanical behaviors of composite hydroxypropyl methylcelluose/zein nanoparticle films. *Food Biophysics*, *13*(1), 25–36. Available from https://doi.org/10.1007/s11483-017-9508-1.

Guo, X., Meng, H., Zhu, S., Zhang, T., & Yu, S. (2015). Purifying sugar beet pectins from non-pectic components by means of metal precipitation. *Food Hydrocolloids*, *51*, 69–75. Available from https://doi.org/10.1016/j.foodhyd.2015.05.009.

Guo, X., Zhao, W., Pang, X., Liao, X., Hu, X., & Wu, J. (2014). Emulsion stabilizing properties of pectins extracted by high hydrostatic pressure, high-speed shearing homogenization and traditional thermal methods: A comparative study. *Food Hydrocolloids*, *35*, 217–225. Available from https://doi.org/10.1016/j.foodhyd.2013.05.010.

Hedayati, S., Shahidi, F., Majzoobi, M., Koocheki, A., & Farahnaky, A. (2020). Structural, rheological, pasting and textural properties of granular cold water swelling maize starch: Effect of NaCl and $CaCl_2$. *Carbohydrate Polymers*, *242*, 116406. Available from https://doi.org/10.1016/j.carbpol.2020.116406.

Hiasa, S., Kumagai, A., Endo, T., & Edashige, Y. (2016). Prevention of aggregation of pectin-containing cellulose nanofibers prepared from mandarin peel. *Journal of Fiber Science and Technology*, 17–26. Available from https://doi.org/10.2115/fiberst.2016-0006.

Hosseini, S. F., Rezaei, M., Zandi, M., & Farahmandghavi, F. (2016). Development of bioactive fish gelatin/chitosan nanoparticles composite films with antimicrobial properties. *Food Chemistry*, *194*, 1266–1274. Available from https://doi.org/10.1016/j.foodchem.2015.09.004.

Huang, T., Tu, Z. c, Wang, H., Shangguan, X., Zhang, L., Zhang, Nh, & Bansal, N. (2017). Pectin and enzyme complex modified fish scales gelatin: Rheological behavior, gel properties and nanostructure. *Carbohydrate Polymers*, *156*, 294–302. Available from https://doi.org/10.1016/j.carbpol.2016.09.040.

Ishii, T., Matsunaga, T., Pellerin, P., O'Neill, M. A., Darvill, A., & Albersheim, P. (1999). The plant cell wall polysaccharide rhamnogalacturonan II self-assembles into a covalently cross-linked dimer. *Journal of Biological Chemistry*, *274*(19), 13098–13104. Available from https://doi.org/10.1074/jbc.274.19.13098.

Javidi, F., Razavi, S. M. A., & Mohammad Amini, A. (2019). Cornstarch nanocrystals as a potential fat replacer in reduced fat O/W emulsions: A rheological and physical study. *Food Hydrocolloids*, *90*, 172–181. Available from https://doi.org/10.1016/j.foodhyd.2018.12.003.

Khorasani, A. C., & Shojaosadati, S. A. (2017). Pectin-non-starch nanofibers biocomposites as novel gastrointestinal-resistant prebiotics. *International Journal of Biological Macromolecules*, *94*, 131–144. Available from https://doi.org/10.1016/j.ijbiomac.2016.10.011.

Kirby, A. R., MacDougall, A. J., & Morris, V. J. (2008). Atomic force microscopy of tomato and sugar beet pectin molecules. *Carbohydrate Polymers*, *71*(4), 640–647. Available from https://doi.org/10.1016/j.carbpol.2007.07.014.

Kocun, M., Grandbois, M., & Cuccia, L. A. (2011). Single molecule atomic force microscopy and force spectroscopy of chitosan. *Colloids and Surfaces B: Biointerfaces*, *82*(2), 470–476. Available from https://doi.org/10.1016/j.colsurfb.2010.10.004.

Kozioł, A., Cybulska, J., Pieczywek, P. M., & Zdunek, A. (2015). Evaluation of structure and assembly of xyloglucan from tamarind seed (Tamarindus indica L.) with atomic

force microscopy. *Food Biophysics*, *10*(4), 396–402. Available from https://doi.org/10.1007/s11483-015-9395-2.

Kozioł, A., Cybulska, J., Pieczywek, P. M., & Zdunek, A. (2017). Changes of pectin nanostructure and cell wall stiffness induced in vitro by pectinase. *Carbohydrate Polymers*, *161*, 197–207. Available from https://doi.org/10.1016/j.carbpol.2017.01.014.

Lai, S., Chen, F., Zhang, L., Yang, H., Deng, Y., & Yang, B. (2013). Nanostructural difference of water-soluble pectin and chelate-soluble pectin among ripening stages and cultivars of Chinese cherryy. *Natural Product Research*, *27*(4–5), 379–385. Available from https://doi.org/10.1080/14786419.2012.696259.

Li, S., Li, J., Zhi, Z., Wei, C., Wang, W., Ding, T., … Chen, S. (2017). Macromolecular properties and hypolipidemic effects of four sulfated polysaccharides from sea cucumbers. *Carbohydrate Polymers*, *173*, 330–337. Available from https://doi.org/10.1016/j.carbpol.2017.05.063.

Li, Y., Zhang, L., Chen, F., Lai, S., & Yang, H. (2018). Effects of vacuum impregnation with calcium ascorbate and disodium stannous citrate on chinese red bayberry. Food and Bioprocess. *Technology (Elmsford, N.Y.)*, *11*(7), 1300–1316. Available from https://doi.org/10.1007/s11947-018-2092-7.

Lin, J., Yu, S., Ai, C., Zhang, T., & Guo, X. (2020). Emulsion stability of sugar beet pectin increased by genipin crosslinking. *Food Hydrocolloids*, *101*, 105459. Available from https://doi.org/10.1016/j.foodhyd.2019.105459.

Lin, M., Deng, Y., Xiao, C., Liu, M., Zhu, L., Luo, W., & Yang, H. (2010). Influence of pure oxygen on nanostructure of water-soluble pectin in pear (Pyrus bretschneideri Rehd cv. Huangguan). *Philippine Agricultural Scientist*, *93*(2), 190–197. Available from http://www.pas-uplbca.edu.ph/downloadPDF.php?file = 008_Min.pdf.

Liu, H., Chen, F., Lai, S., Tao, J., Yang, H., & Jiao, Z. (2017). Effects of calcium treatment and low temperature storage on cell wall polysaccharide nanostructures and quality of postharvest apricot (Prunus armeniaca). *Food Chemistry*, *225*, 87–97. Available from https://doi.org/10.1016/j.foodchem.2017.01.008.

Liu, H., Chen, F., Yang, H., Yao, Y., Gong, X., Xin, Y., & Ding, C. (2009). Effect of calcium treatment on nanostructure of chelate-soluble pectin and physicochemical and textural properties of apricot fruits. *Food Research International*, *42*(8), 1131–1140. Available from https://doi.org/10.1016/j.foodres.2009.05.014.

Liu, J., Tan, J., Hua, X., Jiang, Z., Wang, M., Yang, R., & Cao, Y. (2020). Interfacial properties of ultrahigh methoxylated pectin. *International Journal of Biological Macromolecules*, *152*, 403–410. Available from https://doi.org/10.1016/j.ijbiomac.2020.02.264.

Liu, W., Hu, C., Liu, Y., Dai, S., Lu, W., lv, X., … Gao, X. (2017). Preparation, characterization, and α-glycosidase inhibition activity of a carboxymethylated polysaccharide from the residue of Sarcandra glabra (Thunb.) Nakai. *International Journal of Biological Macromolecules*, *99*, 454–464. Available from https://doi.org/10.1016/j.ijbiomac.2017.02.065.

Magonov, S. N., & Reneker, D. H. (1997). Characterization of polymer surfaces with atomic force microscopy. *Annual Review of Materials Science*, *27*(1), 175–222. Available from https://doi.org/10.1146/annurev.matsci.27.1.175.

Mao, J., Zhang, L., Chen, F., Lai, S., Yang, B., & Yang, H. (2017). Effect of vacuum impregnation combined with calcium lactate on the firmness and polysaccharide morphology of kyoho grapes (Vitis vinifera x V. labrusca). Food and Bioprocess. *Technology (Elmsford, N.Y.)*, *10*(4), 699–709. Available from https://doi.org/10.1007/s11947-016-1852-5.

McIntire, T. M., & Brant, D. A. (1999). Imaging of carrageenan macrocycles and amylose using noncontact atomic force microscopy. *In International Journal of Biological*

Macromolecules, *26*(4), 303–310. Available from https://doi.org/10.1016/S0141-8130(99)00097-5.

Mohnen, D. (2008). Pectin structure and biosynthesis. *Current Opinion in Plant Biology*, *11*(3), 266–277. Available from https://doi.org/10.1016/j.pbi.2008.03.006.

Nagalakshmaiah, M., kissi, N. E., Mortha, G., & Dufresne, A. (2016). Structural investigation of cellulose nanocrystals extracted from chili leftover and their reinforcement in cariflex-IR rubber latex. *Carbohydrate Polymers*, *136*, 945–954. Available from https://doi.org/10.1016/j.carbpol.2015.09.096.

Niimura, H., Yokoyama, T., Kimura, S., Matsumoto, Y., & Kuga, S. (2010). AFM observation of ultrathin microfibrils in fruit tissues. *Cellulose*, *17*(1), 13–18. Available from https://doi.org/10.1007/s10570-009-9361-6.

Ocloo, F. C. K., Ray, S. S., & Emmambux, N. M. (2019). Effects of stearic acid and irradiation alone and in combination on properties of amylose-lipid nanomaterial from high amylose maize starch. *Carbohydrate Polymers*, *212*, 352–360. Available from https://doi.org/10.1016/j.carbpol.2019.02.065.

Paniagua, C., Kirby, A. R., Gunning, A. P., Morris, V. J., Matas, A. J., Quesada, M. A., & Mercado, J. A. (2017). Unravelling the nanostructure of strawberry fruit pectins by *endo*-polygalacturonase digestion and atomic force microscopy. *Food Chemistry*, *224*, 270–279. Available from https://doi.org/10.1016/j.foodchem.2016.12.049.

Paniagua, C., Posé, S., Morris, V. J., Kirby, A. R., Quesada, M. A., & Mercado, J. A. (2014). Fruit softening and pectin disassembly: An overview of nanostructural pectin modifications assessed by atomic force microscopy. *Annals of Botany*, *114*(6), 1375–1383. Available from https://doi.org/10.1093/aob/mcu149.

Peroni-Okita, F. H. G., Gunning, A. P., Kirby, A., Simão, R. A., Soares, C. A., & Cordenunsi, B. R. (2015). Visualization of internal structure of banana starch granule through AFM. *Carbohydrate Polymers*, *128*, 32–40. Available from https://doi.org/10.1016/j.carbpol.2015.04.019.

Pieczywek, P. M., Kozioł, A., Konopacka, D., Cybulska, J., & Zdunek, A. (2017). Changes in cell wall stiffness and microstructure in ultrasonically treated apple. *Journal of Food Engineering*, *197*, 1–8. Available from https://doi.org/10.1016/j.jfoodeng.2016.10.028.

Pieczywek, P. M., Kozioł, A., Płaziński, W., Cybulska, J., & Zdunek, A. (2020). Resolving the nanostructure of sodium carbonate extracted pectins (DASP) from apple cell walls with atomic force microscopy and molecular dynamics. *Food Hydrocolloids*, *104*, 105726. Available from https://doi.org/10.1016/j.foodhyd.2020.105726.

Posé, S., Paniagua, C., Matas, A. J., Gunning, A. P., Morris, V. J., Quesada, M. A., & Mercado, J. A. (2019). A nanostructural view of the cell wall disassembly process during fruit ripening and postharvest storage by atomic force microscopy. *Trends in Food Science and Technology*, *87*, 47–58. Available from https://doi.org/10.1016/j.tifs.2018.02.011.

Radziejewska-Kubzdela, E., Biegańska-Marecik, R., & Kidoń, M. (2014). Applicability of vacuum impregnation to modify physico-chemical, sensory and nutritive characteristics of plant origin products—A review. *International Journal of Molecular Sciences*, *15*(9), 16577–16610. Available from https://doi.org/10.3390/ijms150916577.

Ren, Z., Li, Z., Chen, Z., Zhang, Y., Lin, X., Wang, W., … Li, B. (2021). Characteristics and application of fish oil-in-water pickering emulsions structured with tea water-insoluble proteins/κ-carrageenan complexes. *Food Hydrocolloids*, *114*, 106562. Available from https://doi.org/10.1016/j.foodhyd.2020.106562.

Ridout, M. J., Gunning, A. P., Parker, M. L., Wilson, R. H., & Morris, V. J. (2002). Using AFM to image the internal structure of starch granules. *Carbohydrate Polymers*, *50*(2), 123–132. Available from https://doi.org/10.1016/S0144-8617(02)00021-8.

Ridout, M. J., Parker, M. L., Hedley, C. L., Bogracheva, T. Y., & Morris, V. J. (2003). Atomic force microscopy of pea starch granules: Granule architecture of wild-type

parent, r and rb single mutants, and the rrb double mutant. *Carbohydrate Research*, *338* (20), 2135–2147. Available from https://doi.org/10.1016/S0008-6215(03)00309-4.

Singh, S., Nwabor, O. F., Ontong, J. C., Kaewnopparat, N., & Voravuthikunchai, S. P. (2020). Characterization of a novel, co-processed bio-based polymer, and its effect on mucoadhesive strength. *International Journal of Biological Macromolecules*, *145*, 865–875. Available from https://doi.org/10.1016/j.ijbiomac.2019.11.198.

Sletmoen, M., Maurstad, G., Sikorski, P., Paulsen, B. S., & Stokke, B. T. (2003). Characterisation of bacterial polysaccharides: Steps towards single-molecular studies. *Carbohydrate Research*, *338*(23), 2459–2475. Available from https://doi.org/10.1016/j.carres.2003.07.007.

Sow, L. C., Nicole Chong, J. M., Liao, Q. X., & Yang, H. (2018). Effects of κ-carrageenan on the structure and rheological properties of fish gelatin. *Journal of Food Engineering*, *239*, 92–103. Available from https://doi.org/10.1016/j.jfoodeng.2018.05.035.

Sujka, M., & Jamroz, J. (2009). α-Amylolysis of native potato and corn starches - SEM, AFM, nitrogen and iodine sorption investigations. *LWT - Food Science and Technology*, *42*(7), 1219–1224. Available from https://doi.org/10.1016/j.lwt.2009.01.016.

Szymańska-Chargot, M., Chylińska, M., Cybulska, J., Kozioł, A., Pieczywek, P. M., & Zdunek, A. (2017). Simultaneous influence of pectin and xyloglucan on structure and mechanical properties of bacterial cellulose composites. *Carbohydrate Polymers*, *174*, 970–979. Available from https://doi.org/10.1016/j.carbpol.2017.07.004.

Szymańska-Chargot, M., Chylińska, M., Gdula, K., Kozioł, A., & Zdunek, A. (2017). Isolation and characterization of cellulose from different fruit and vegetable pomaces. *Polymers*, *9*(10), 495. Available from https://doi.org/10.3390/polym9100495.

Tappi, S., Tylewicz, U., Romani, S., Siroli, L., Patrignani, F., Dalla Rosa, M., & Rocculi, P. (2016). Optimization of vacuum impregnation with calcium lactate of minimally processed melon and shelf-life study in real storage conditions. *Journal of Food Science*, *81*(11), E2734–E2742. Available from https://doi.org/10.1111/1750-3841.13513.

Tavallaie, S., Khomeiri, M., Mousivand, M., Maghsoudlou, Y., & Hashemi, M. (2019). Starches from different sources hydrolysis using a new thermo-tolerant amylase complex produced by Bacillus subtilis T41a: Characterization and efficiency evaluation. *LWT*, *112*, 108218. Available from https://doi.org/10.1016/j.lwt.2019.05.116.

Teckentrup, J., Al-Hammood, O., Steffens, T., Bednarz, H., Walhorn, V., Niehaus, K., & Anselmetti, D. (2017). Comparative analysis of different xanthan samples by atomic force microscopy. *Journal of Biotechnology*, *257*, 2–8. Available from https://doi.org/10.1016/j.jbiotec.2016.11.032.

Venkateshaiah, A., Padil, V. V. T., Nagalakshmaiah, M., Waclawek, S., Černík, M., & Varma, R. S. (2020). Microscopic techniques for the analysis of micro and nanostructures of biopolymers and their derivatives. *Polymers*, *12*(3). Available from https://doi.org/10.3390/polym12030512.

Vincken, J. P., Schols, H. A., Oomen, R. J. F. J., McCann, M. C., Ulvskov, P., Voragen, A. G. J., & Visser, R. G. F. (2003). If homogalacturonan were a side chain of rhamnogalacturonan I. Implications for cell wall architecture. *Plant Physiology*, *132*(4), 1781–1789. Available from https://doi.org/10.1104/pp.103.022350.

Wang, H., Chen, F., Yang, H., Chen, Y., Zhang, L., & An, H. (2012). Effects of ripening stage and cultivar on physicochemical properties and pectin nanostructures of jujubes. *Carbohydrate Polymers*, *89*(4), 1180–1188. Available from https://doi.org/10.1016/j.carbpol.2012.03.092.

Wang, H., Fei, S., Wang, Y., Zan, L., & Zhu, J. (2020). Comparative study on the self-assembly of pectin and alginate molecules regulated by calcium ions investigated by atomic force microscopy. *Carbohydrate Polymers*, *231*, 115673. Available from https://doi.org/10.1016/j.carbpol.2019.115673.

Wang, L., Xiang, D., Li, C., Zhang, W., & Bai, X. (2021). Effects of lyophilization and low-temperature treatment on the properties and conformation of xanthan gum. *Food Hydrocolloids*, *112*, 106352. Available from https://doi.org/10.1016/j.foodhyd.2020.106352.

Wen, Y., Xu, Z., Liu, Y., Corke, H., & Sui, Z. (2020). Investigation of food microstructure and texture using atomic force microscopy: A review. *Comprehensive Reviews in Food Science and Food Safety*, *19*(5), 2357–2379. Available from https://doi.org/10.1111/1541-4337.12605.

Willats, W. G. T., Knox, J. P., & Mikkelsen, J. D. (2006). Pectin: New insights into an old polymer are starting to gel. *Trends in Food Science and Technology*, *17*(3), 97–104. Available from https://doi.org/10.1016/j.tifs.2005.10.008.

Willats, W. G. T., Mccartney, L., Mackie, W., & Knox, J. P. (2001). Pectin: Cell biology and prospects for functional analysis. *Plant Molecular Biology*, *47*(1–2), 9–27. Available from https://doi.org/10.1023/A:1010662911148.

Xin, Y., Chen, F., Yang, H., Zhang, P., Deng, Y., & Yang, B. (2010). Morphology, profile and role of chelate-soluble pectin on tomato properties during ripening. *Food Chemistry*, *121*(2), 372–380. Available from https://doi.org/10.1016/j.foodchem.2009.12.038.

Xin, Y., Jin, Z., Chen, F., Lai, S., & Yang, H. (2020). Effect of chitosan coatings on the evolution of sodium carbonate-soluble pectin during sweet cherry softening under non-isothermal conditions. *International Journal of Biological Macromolecules*, *154*, 267–275. Available from https://doi.org/10.1016/j.ijbiomac.2020.03.104.

Yang, D., & Yang, H. (2020). The temperature dependent extraction of polysaccharides from eucheuma and the rheological synergistic effect in their mixtures with kappa carrageenan. *LWT*, *129*, 109515. Available from https://doi.org/10.1016/j.lwt.2020.109515.

Yang, H., An, H., Feng, G., & Li, Y. (2005). Visualization and quantitative roughness analysis of peach skin by atomic force microscopy under storage. *LWT – Food Science and Technology*, *38*(6), 571–577. Available from https://doi.org/10.1016/j.lwt.2004.09.007.

Yang, H., An, H., Feng, G., Li, Y., & Lai, S. (2005). Atomic force microscopy of the water-soluble pectin of peaches during storage. *European Food Research and Technology*, *220*(5–6), 587–591. Available from https://doi.org/10.1007/s00217-004-1102-3.

Yang, H., Chen, F., An, H., & Lai, S. (2009). Comparative studies on nanostructures of three kinds of pectins in two peach cultivars using atomic force microscopy. *Postharvest Biology and Technology*, *51*(3), 391–398. Available from https://doi.org/10.1016/j.postharvbio.2008.08.009.

Yang, H., Lai, S., An, H., & Li, Y. (2006). Atomic force microscopy study of the ultrastructural changes of chelate-soluble pectin in peaches under controlled atmosphere storage. *Postharvest Biology and Technology*, *39*(1), 75–83. Available from https://doi.org/10.1016/j.postharvbio.2005.08.001.

Yang, H., Wu, Q., Ng, L. Y., & Wang, S. (2017). Effects of vacuum impregnation with calcium lactate and pectin methylesterase on quality attributes and chelate-soluble pectin morphology of fresh-cut papayas. Food and Bioprocess. *Technology (Elmsford, N. Y.)*, *10*(5), 901–913. Available from https://doi.org/10.1007/s11947-017-1874-7.

Yang, H. S., Feng, G. P., An, H. J., & Li, Y. F. (2006). Microstructure changes of sodium carbonate-soluble pectin of peach by AFM during controlled atmosphere storage. *Food Chemistry*, *94*(2), 179–192. Available from https://doi.org/10.1016/j.foodchem.2004.11.003.

Yang, L., & Zhang, L. M. (2009). Chemical structural and chain conformational characterization of some bioactive polysaccharides isolated from natural sources. *Carbohydrate Polymers*, *76*(3), 349–361. Available from https://doi.org/10.1016/j.carbpol.2008.12.015.

Yang, Z., Xu, X., Singh, R., de Campo, L., Gilbert, E. P., Wu, Z., & Hemar, Y. (2019). Effect of amyloglucosidase hydrolysis on the multi-scale supramolecular structure of corn starch. *Carbohydrate Polymers*, *212*, 40–50. Available from https://doi.org/10.1016/j.carbpol.2019.02.028.

Ye, J., Hua, X., Zhao, Q., Zhao, W., Chu, G., Zhang, W., & Yang, R. (2020). Chain conformation and rheological properties of an acid-extracted polysaccharide from peanut sediment of aqueous extraction process. *Carbohydrate Polymers*, *228*, 115410. Available from https://doi.org/10.1016/j.carbpol.2019.115410.

Yusof, N. L., Wadsö, L., Rasmusson, A. G., & Gómez Galindo, F. (2017). Influence of vacuum impregnation with different substances on the metabolic heat production and sugar metabolism of spinach leaves. *Food and Bioprocess Technology*, *10*(10), 1907–1917. Available from https://doi.org/10.1007/s11947-017-1959-3.

Zdunek, A., Kozioł, A., Cybulska, J., Lekka, M., & Pieczywek, P. M. (2016). The stiffening of the cell walls observed during physiological softening of pears. *Planta*, *243*(2), 519–529. Available from https://doi.org/10.1007/s00425-015-2423-0.

Zdunek, A., Kozioł, A., Pieczywek, P. M., & Cybulska, J. (2014). Evaluation of the nanostructure of pectin, hemicellulose and cellulose in the cell walls of pears of different texture and firmness. Food and Bioprocess. *Technology (Elmsford, N.Y.)*, 7(12), 3525–3535. Available from https://doi.org/10.1007/s11947-014-1365-z.

Zhang, H., Chen, J., Li, J., Yan, L., Li, S., Ye, X., … Chen, S. (2018). Extraction and characterization of RG-I enriched pectic polysaccharides from mandarin citrus peel. *Food Hydrocolloids*, *79*, 579–586. Available from https://doi.org/10.1016/j.foodhyd.2017.12.002.

Zhang, J., Cui, J., Xiao, L., & Wang, Z. (2014). The combination of atomic force microscopy and sugar analysis to evaluate alkali-soluble Canna edulis Ker pectin. *Food Chemistry*, *156*, 64–71. Available from https://doi.org/10.1016/j.foodchem.2014.01.096.

Zhang, L., Chen, F., An, H., Yang, H., Sun, X., Guo, X., & Li, L. (2008). Physicochemical properties, firmness, and nanostructures of sodium carbonate-soluble pectin of 2 chinese cherry cultivars at 2 ripening stages. *Journal of Food Science*, *73*(6), N17–N22. Available from https://doi.org/10.1111/j.1750-3841.2008.00799.x.

Zhang, L., Chen, F., Lai, S., Wang, H., & Yang, H. (2018). Impact of soybean protein isolate-chitosan edible coating on the softening of apricot fruit during storage. *LWT*, *96*, 604–611. Available from https://doi.org/10.1016/j.lwt.2018.06.011.

Zhang, L., Chen, F., Yang, H., Sun, X., Liu, H., Gong, X., … Ding, C. (2010). Changes in firmness, pectin content and nanostructure of two crisp peach cultivars after storage. *LWT - Food Science and Technology*, *43*(1), 26–32. Available from https://doi.org/10.1016/j.lwt.2009.06.015.

Zhang, L., Chen, F., Yang, H., Ye, X., Sun, X., Liu, D., … Deng, Y. (2012). Effects of temperature and cultivar on nanostructural changes of water-soluble pectin and chelate-soluble pectin in peaches. *Carbohydrate Polymers*, *87*(1), 816–821. Available from https://doi.org/10.1016/j.carbpol.2011.08.074.

Zhang, L., Chen, F., Zhang, P., Lai, S., & Yang, H. (2017). Influence of rice bran wax coating on the physicochemical properties and pectin nanostructure of cherry tomatoes. Food and Bioprocess. *Technology (Elmsford, N.Y.)*, *10*(2), 349–357. Available from https://doi.org/10.1007/s11947-016-1820-0.

Zhang, L., Wang, P., Chen, F., Lai, S., Yu, H., & Yang, H. (2019). Effects of calcium and pectin methylesterase on quality attributes and pectin morphology of jujube fruit under vacuum impregnation during storage. *Food Chemistry*, *289*, 40–48. Available from https://doi.org/10.1016/j.foodchem.2019.03.008.

Zhang, L., Wang, P., Sun, X., Chen, F., Lai, S., & Yang, H. (2020). Calcium permeation property and firmness change of cherry tomatoes under ultrasound combined with

calcium lactate treatment. *Ultrasonics Sonochemistry*, *60*, 104784. Available from https://doi.org/10.1016/j.ultsonch.2019.104784.

Zhang, L., Ye, X., Xue, S. J., Zhang, X., Liu, D., Meng, R., & Chen, S. (2013). Effect of high-intensity ultrasound on the physicochemical properties and nanostructure of citrus pectin. *Journal of the Science of Food and Agriculture*, *93*(8), 2028–2036. Available from https://doi.org/10.1002/jsfa.6011.

Zhang, L., Zhang, X., Liu, D., Ding, T., & Ye, X. (2015). *Effect of degradation methods on the structural properties of citrus pectin*. *LWT - Food Science and Technology*, *61*(2), 630–637. Available from https://doi.org/10.1016/j.lwt.2014.11.002.

Zhang, L., Zhao, S., Lai, S., Chen, F., & Yang, H. (2018). Combined effects of ultrasound and calcium on the chelate-soluble pectin and quality of strawberries during storage. *Carbohydrate Polymers*, *200*, 427–435. Available from https://doi.org/10.1016/j.carbpol.2018.08.013.

Zhang, T., Zheng, Y., & Cosgrove, D. J. (2016). Spatial organization of cellulose microfibrils and matrix polysaccharides in primary plant cell walls as imaged by multichannel atomic force microscopy. *Plant Journal*, *85*(2), 179–192. Available from https://doi.org/10.1111/tpj.13102.

Zhang, W., Fan, X., Gu, X., Gong, S., Wu, J., Wang, Z., … Wang, S. (2020). Emulsifying properties of pectic polysaccharides obtained by sequential extraction from black tomato pomace. *Food Hydrocolloids*, *100*, 105454. Available from https://doi.org/10.1016/j.foodhyd.2019.105454.

Zhang, X., Lin, J., Pi, F., Zhang, T., Ai, C., & Yu, S. (2020). Rheological characterization of RG-I chicory root pectin extracted by hot alkali and chelators. *International Journal of Biological Macromolecules*, *164*, 759–770. Available from https://doi.org/10.1016/j.ijbiomac.2020.07.020.

Zhi, H., Liu, Q., Xu, J., Dong, Y., Liu, M., & Zong, W. (2017). Ultrasound enhances calcium absorption of jujube fruit by regulating the cellular calcium distribution and metabolism of cell wall polysaccharides. *Journal of the Science of Food and Agriculture*, *97*(15), 5202–5210. Available from https://doi.org/10.1002/jsfa.8402.

Zlatanova, J., & van Holde, K. (2006). Single-molecule biology: What is it and how does it work? *Molecular Cell*, *24*(3), 317–329. Available from https://doi.org/10.1016/j.molcel.2006.10.017.

Zlatanova, J., & Leuba, S. H. (2002). Stretching and imaging single DNA molecules and chromatin. *Journal of Muscle Research and Cell Motility*, *23*(5–6), 377–395. Available from https://doi.org/10.1023/A:1023498120458.

Further reading

Liu, D., & Cheng, F. (2011). Advances in research on structural characterisation of agricultural products using atomic force microscopy. *Journal of the Science of Food and Agriculture*, *91*(5), 783–788. Available from https://doi.org/10.1002/jsfa.4284.